bioRxiv preprint doi: https://doi.org/10.1101/2021.02.24.432727; this version posted February 24, 2021. The copyright holder for this preprint (which was not certified by peer review) is the author/funder. All rights reserved. No reuse allowed without permission.

Transport Dynamics of MtrD: an RND multidrug efflux pump from *Neisseria gonorrhoeae*

Lauren Ammerman[1,2,3*], Sarah B. Mertz [1,2,3], Chanyang Park[1,3], and John G. Wise[1,2,3*]

[1] Department of Biological Sciences, [2] Center for Scientific Computation, [3]Center for Drug Discovery, Design and Delivery; Southern Methodist University, Dallas, TX 75275

* Corresponding authors

E-mail: jwise@smu.edu, lammerman@smu.edu

bioRxiv preprint doi: https://doi.org/10.1101/2021.02.24.432727; this version posted February 24, 2021. The copyright holder for this preprint (which was not certified by peer review) is the author/funder. All rights reserved. No reuse allowed without permission.

Abstract

Antibiotic-resistant gonorrheal infections are an urgent health concern. The MtrCDE system confers multidrug resistance to *Neisseria gonorrhoeae*, an obligate human pathogen, and the causative agent of the sexually-transmitted infection gonorrhea. The inner membrane pump MtrD effluxes a variety of hydrophobic and amphiphilic substrates and thereby confers resistance to a multitude of antibiotics. Using a combination of free and directed Molecular Dynamics (MD) simulations, we analyzed the interactions of MtrD with Azithromycin, an MtrD substrate and one of the last remaining courses of treatment for multidrug resistant gonorrhea. We also simulated the interactions between MtrD and Streptomycin, a non-substrate of MtrD. Using targeted MD (TMD) techniques and known conformations of MtrD homologues, we guided MtrD through the conformational changes of a putative transport cycle by applying small forces to α-carbons of the protein backbone; forces were not applied to Azithromycin or to Streptomycin. In our TMD experiments, we observed the transport of Azithromycin (in three possible protonation states) and the rejection of Streptomycin. To supplement our findings, we then demonstrate the spontaneous diffusion of Azithromycin through the periplasmic cleft in long time-scale, unbiased MD simulations. Our findings support the hypothesis that the transition from 'Binding' to 'Extrusion' is an energy requiring step in the transport process. Our data also suggest that multiple binding modes, and potentially multiple residue contact pathways, exist within the periplasmic cleft of MtrD, even for bulky substrates. To our knowledge, this is the first computational demonstration of substrate transport, and non-substrate rejection, by MtrD.

bioRxiv preprint doi: https://doi.org/10.1101/2021.02.24.432727; this version posted February 24, 2021. The copyright holder for this preprint (which was not certified by peer review) is the author/funder. All rights reserved. No reuse allowed without permission.

Introduction

The gram-negative diplococcus *Neisseria gonorrhoeae* is responsible for the sexually transmitted infection (STI) Gonorrhea, and with over 87 million cases of Gonorrhea reported worldwide, antibiotic resistance in *N. gonorrhoeae* is a global health concern [1, 2]. *N. gonorrhoeae* is an obligate human pathogen that can cause severe reproductive and general health complications, if left untreated [2]. The number of effective antibiotics against *N. gonorrhoeae* is dwindling, and for multidrug resistant gonorrheal infections, only one recommended treatment remains – a combination treatment with the antibiotics ceftriaxone and azithromycin [2]. Unfortunately, a strain of *N. gonorrhoeae* with resistance to both azithromycin and ceftriaxone was detected in 2018 [3]. It remains increasingly important to understand and target the mechanisms that confer antibiotic resistance to *N. gonorrhoeae*.

Gram negative pathogens like *N. gonorrhoeae* have evolved several intricate mechanisms to overcome antimicrobial attack, and among the most effective are the resistance, nodulation and cell-division (RND) efflux systems [4]. These tripartite protein complexes consist of an efflux pump embedded in the inner membrane, a channel that passes through the outer membrane, and a periplasmic adaptor that connects the pump and channel through the periplasmic space. While four efflux pump systems have been identified in *N. gonorrhoeae* – MtrCDE, MacAB, NorM, and FarAB [5], the best characterized system is the multiple transferrable resistance, MtrCDE system, which consists of the MtrD inner membrane pump, the MtrC periplasmic adaptor, and the MtrE outer membrane channel [6-8]. A member of the HAE (Hydrophobic and Amphiphilic Efflux) family, MtrD exports bile salts, antimicrobial peptides, dyes, β-lactams, and macrolides [7, 9]. Overexpression of MtrCDE contributes significantly to clinical levels of macrolide resistance in *N. gonorrhoeae* [8, 10]. In mouse infection models, expression of active MtrCDE has been shown to be critical for gonococcal survival [11, 12]. Lastly, mutations in the drug binding region of MtrD are correlated with changes in antibiotic resistance in *N. gonorrhoeae* [9]. Given its importance in virulence and multiple antibiotic resistances, the MtrD efflux pump remains a promising target for the development of therapeutics.

MtrD assembles as a homotrimer, with each protomer consisting of a large periplasmic domain and 12 transmembrane helices [6, 13] (Fig 1A). The periplasmic domain contains the periplasmic cleft, which

bioRxiv preprint doi: https://doi.org/10.1101/2021.02.24.432727; this version posted February 24, 2021. The copyright holder for this preprint (which was not certified by peer review) is the author/funder. All rights reserved. No reuse allowed without permission.

is responsible for the capture and extrusion of substrates, as well as the docking domain that interfaces with MtrCE (Figure 1B). The periplasmic cleft is further divided into the PN1, PN2, PC1, and PC2 domains; these create the proximal and distal multidrug binding sites (also known as the Access Pocket and the Deep Pocket, respectively), and are bisected by a flexible and conserved G-Loop (Fig 1C). The transmembrane helices house a highly conserved residue network that utilizes the proton-motive-force across the bacterial plasma membrane to power the pump [6] (Fig 1D). Changes in the protonation state(s) of these residues are thought to result in shearing motions of the TM helices, which correlate with peristaltic motions of the periplasmic cleft and thereby facilitate the movement of a substrate though the cleft [14, 15]. Substrates of large molecular weight are thought to bind first to the proximal binding site in the Access Pocket, and then second to the distal binding site in the Deep Pocket, before extrusion occurs through the funnel created by the docking domains of the homotrimer [6, 13]. The composition of the proximal and distal binding sites has been defined by some mutational studies (which identified residues 714 and 823 as important for macrolide recognition [13] and by co-crystal structures of erythromycin [16]. The transmembrane helices of each protomer house the highly conserved proton-relay-network (PRN, Fig 1D) [13].

bioRxiv preprint doi: https://doi.org/10.1101/2021.02.24.432727; this version posted February 24, 2021. The copyright holder for this preprint (which was not certified by peer review) is the author/funder. All rights reserved. No reuse allowed without permission.

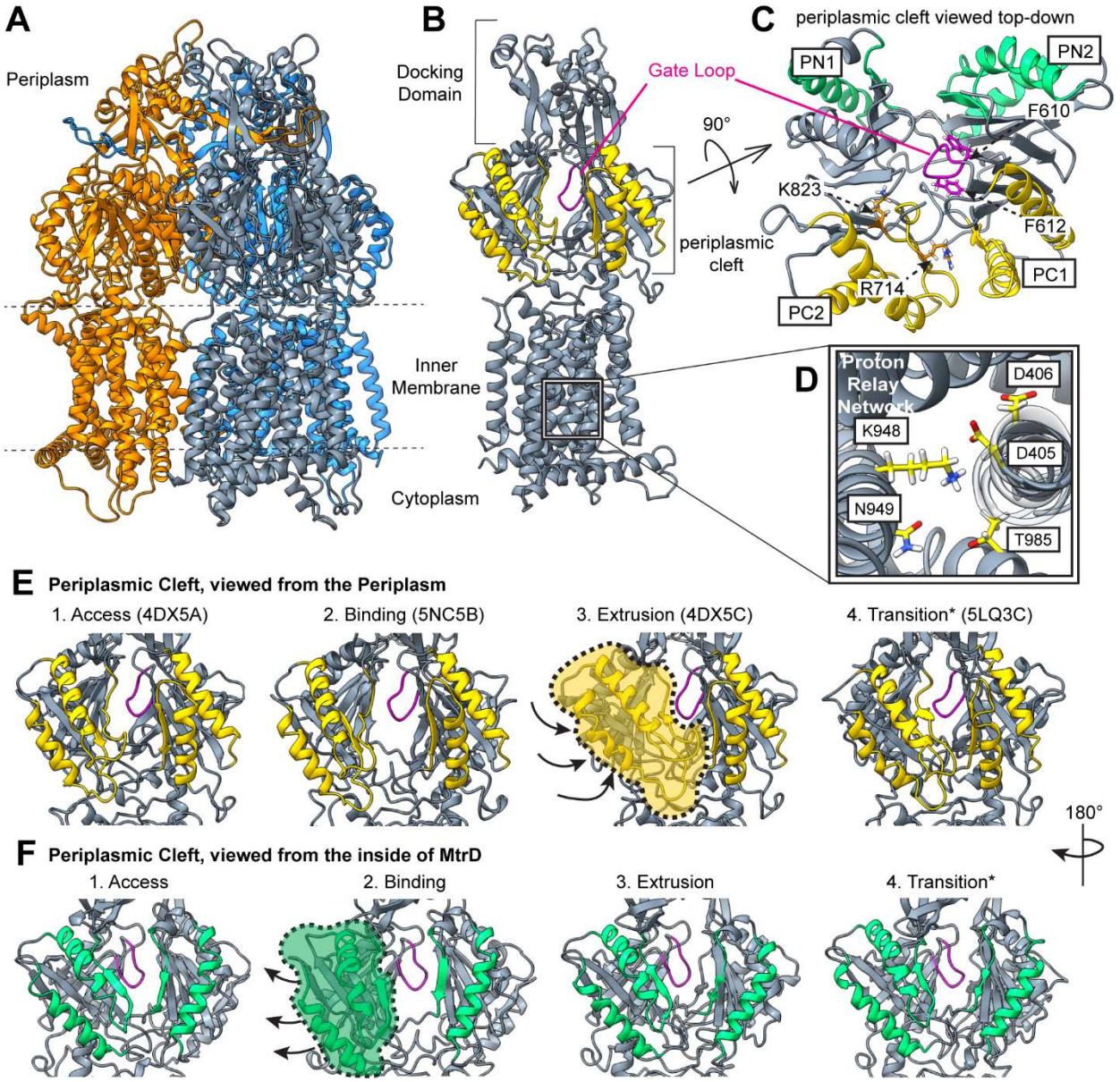

Fig 1. The MtrD Efflux Pump from *Neisseria gonorrhoeae*. (A) The MtrD homotrimer with subunits colored orange, gray and blue. (B) An MtrD monomer with helices of the Access Pocket in yellow and the G-Loop in magenta. (C) The periplasmic cleft viewed as if looking from the periplasm towards the inner membrane; helices of the Access Pocket in yellow, helices of the Deep Pocket in green, G-Loop in magenta. K823 and R714 may contribute to macrolide recognition (in orange sticks), and F612 and F610 may facilitate substrate selectivity [13]. (D) The Proton Relay Network. (E) The Access Pocket viewed from the periplasm; arrows show how PC2 (shaded yellow) closes during the transport cycle. (F) The Deep Pocket viewed from the central pore; arrows show how PN2 (shaded green) opens during the transport cycle. Stages of the transport cycle are labeled Access (also 'Loose'), Binding ('Tight'), Extrusion ('Open'), and Intermediate with the corresponding crystal structure of the MtrD homologue AcrB (5NC5, 4DX5) or CmeB (5LQ3) in parentheses [6, 17]. Helices of the Access or Deep Pockets are colored differentially to aid in the visualization of conformational changes during the transport process.

To transport a substrate, it is thought that MtrD undergoes a sequence of conformational changes, resulting in shifting of its transmembrane helices and what might be thought of as a peristalsis-like motion

bioRxiv preprint doi: https://doi.org/10.1101/2021.02.24.432727; this version posted February 24, 2021. The copyright holder for this preprint (which was not certified by peer review) is the author/funder. All rights reserved. No reuse allowed without permission.

of the Drug Binding Pocket (Figs 1E-F,S1). Several distinct conformations of RND pumps have been identified by structural studies. When these conformations are sequenced in an order that may make sense in terms of a catalytic cycle, they are (1) 'Access/Loose', (2) 'Binding/Tight' (3) 'Extrusion/Open', and potentially a (4) Resting/Intermediate' conformation, which may be a transition structure from Extrusion back to Access (Fig 1E,F) [13, 17-20]. Substrate-free MtrD adopts a symmetrical conformation with each protomer in the Access state [6]. Upon the binding of a transport substrate to an Access protomer, the trimer adopts an asymmetric conformation in which each of the three protomers adopts one of the conformational states – Access, Binding, or Extrusion [13, 18]. During the transition from Access to Binding, the substrate is thought to move from the Access Pocket to the Deep Pocket [13, 14]. Each monomer of MtrD subsequently cycles from Access, to Binding, to Extrusion in a functional rotation mechanism [14]. It has been shown that the characteristics of the Drug Binding Pocket may contribute to the substrate specificity of the pump, and that some of these features change during the transport process [13, 21]. While these known conformational changes provide a framework for understanding the overall movement of the protein during a catalytic transport cycle, the process by which these conformations and conformational changes result in the recognition, movement and extrusion of a substrate is not well understood.

To understand the process of drug transport by MtrD, we simulated the interactions between wild-type MtrD and two antibiotics: azithromycin, a substrate of MtrD, and streptomycin, a non-substrate of MtrD [7, 9]. Through a combination of free and directed Molecular Dynamics (MD) simulations, we simulated a putative dynamic efflux cycle using the known conformations of MtrD homologues as targets. In our Targeted Molecular Dynamics (TMD) simulations, small forces were applied to a subset of α-carbons of the MtrD backbone, but not to any other atoms of the protein or to the ligands of interest. Since substrates are thought to bind sequentially to the proximal and distal binding sites in the periplasmic cleft [6], we tested three start sites for each ligand – a proximal site, a distal site, and a site in-between the proximal and distal sites. To account for the different protonation states of azithromycin that may occur at physiological pH, we simulated each of the three states; it should be noted that only one protonation state of streptomycin occurs at physiological pH. Lastly, we tested the effect of including a fourth Intermediate conformation in the sequence after the known Access, Binding, and Extrusion states. To confirm our findings in these short

bioRxiv preprint doi: https://doi.org/10.1101/2021.02.24.432727; this version posted February 24, 2021. The copyright holder for this preprint (which was not certified by peer review) is the author/funder. All rights reserved. No reuse allowed without permission.

timescale, non-equilibrium simulations, we performed a 1.5 µs equilibrium simulation of azithromycin and MtrD. This long time-scale simulation was performed using AMBER18 and the pmemd.cuda-DPFP molecular dynamics engine [22, 23]. All TMD experiments were performed using NAMD with CHARMM36 force fields [24-27].

In the TMD simulations, we observed the transport of azithromycin and the rejection of streptomycin by MtrD. We show that the molecular landscape of the periplasmic cleft changes dynamically to facilitate substrate discrimination, transport and extrusion. In contrast to results from crystal structures of the MtrD homologue AcrB and cryo-EM structures of $MtrD_{CR103}$, a variant that confers elevated azithromycin resistance, azithromycin was not observed in our TMD simulations to interact with residues of the putative distal binding site as expected, but took an alternate transport pathway mediated by water and polar interactions [13, 16]. In our TMD simulations, we also observed that including a putative fourth Intermediate structure increases the distance that azithromycin moves through MtrD. In an unconstrained 1.5 µs MD simulation (biasing forces were not applied) of azithromycin-bound MtrD in the Access conformation, we observed the spontaneous movement of azithromycin past the G-Loop and into the Deep Pocket. In this long timescale simulation, we note that the movement of azithromycin, and conformational changes of the periplasmic cleft, occurred in the absence of any biasing forces or changes to the Proton Relay Network. Lastly, to explore the potential role of the membrane fusion protein MtrC, we built a full MtrCDE complex using a combination of known structures and molecular modeling.

Taken together, our data suggest that multiple pathways through the periplasmic cleft may exist — even for bulky macrolide substrates like azithromycin. Our data also indicate that MtrC may not play an active role in substrate capture and extrusion, but suggest that a unique feature of MtrD, the TM9 helix and TM9-TM10 linker, might play a role in the capture of amphiphilic substrates from the inner membrane-periplasmic interface. Lastly, our results support the hypothesis that the transition from Binding to Extrusion is an energy-requiring step in the transport process.

bioRxiv preprint doi: https://doi.org/10.1101/2021.02.24.432727; this version posted February 24, 2021. The copyright holder for this preprint (which was not certified by peer review) is the author/funder. All rights reserved. No reuse allowed without permission.

Results

Using Targeted Molecular Dynamics (TMD) simulations directed by known, low energy conformations derived from biophysically determined structures of MtrD homologues, we simulated the putative catalytic transport cycle of MtrD by applying small forces to the α-carbons of the protein backbone to move MtrD through a putative catalytic cycle (Figs 1E,F, S1). As ligands for our MD simulations, we chose the MtrD substrate, azithromycin (AZY), and the MtrD non-substrate, streptomycin (SRY) [7, 9].

Positioning ligands to generate starting sites for TMD simulations

The periplasmic cleft of MtrD can be divided into the Access Pocket and the Deep Pocket, which are composed of the PC1/PC2 domains and the PN1/PN2 domains, respectively (Fig 2A) [9, 16, 21]. Within the Access and Deep Pockets are the putative proximal and distal binding sites of MtrD (Fig 2A). The proximal binding site of MtrD has been proposed to consist of charged, polar and hydrophobic residues from PC1, PC2 and PN2, (Fig 2A,B), while the distal binding site is thought to be composed of mostly hydrophobic residues from PC1 and PN2 (Fig 2A,C) [6, 13]. Structures of the homologous RND transporter AcrB suggest that large substrates first bind to the Access Pocket, and then subsequently pass the G-Loop into the Deep Pocket during the transition from the Access to the Binding conformation (Fig 1C,E,F) [13, 16]. It should be noted that there is an alternative entry site at the PC1/PN2 cleft for small, hydrophobic substrates (Fig 2A), but due to their large sizes, both SRY and AZY (~581 Daltons, ~749 Daltons, respectively) cannot utilize this alternative entry site and must enter the periplasmic cleft through the Access Pocket.

Structures of AcrB indicate that erythromycin, which is quite similar to AZY, may bind at the entrance of the periplasmic cleft [16]. As shown in Fig 2B and 2C, several residues of the MtrD proximal binding site (residues in orange) are conserved in AcrB, two of which (K714 and K823) are thought to contribute to recognition of macrolides like erythromycin and azithromycin [13]. Due to a dearth of structural data, the exact binding location of AZY or SRY in the proximal binding site of MtrD remains unclear [13]. It is reasonable to assume that AZY might interact with the same residues of the MtrD proximal site as erythromycin. However, as we discuss later in this paper, the Access Pocket – and the

bioRxiv preprint doi: https://doi.org/10.1101/2021.02.24.432727; this version posted February 24, 2021. The copyright holder for this preprint (which was not certified by peer review) is the author/funder. All rights reserved. No reuse allowed without permission.

proximal site within – are large enough to accommodate multiple binding modes of azithromycin, despite its large size.

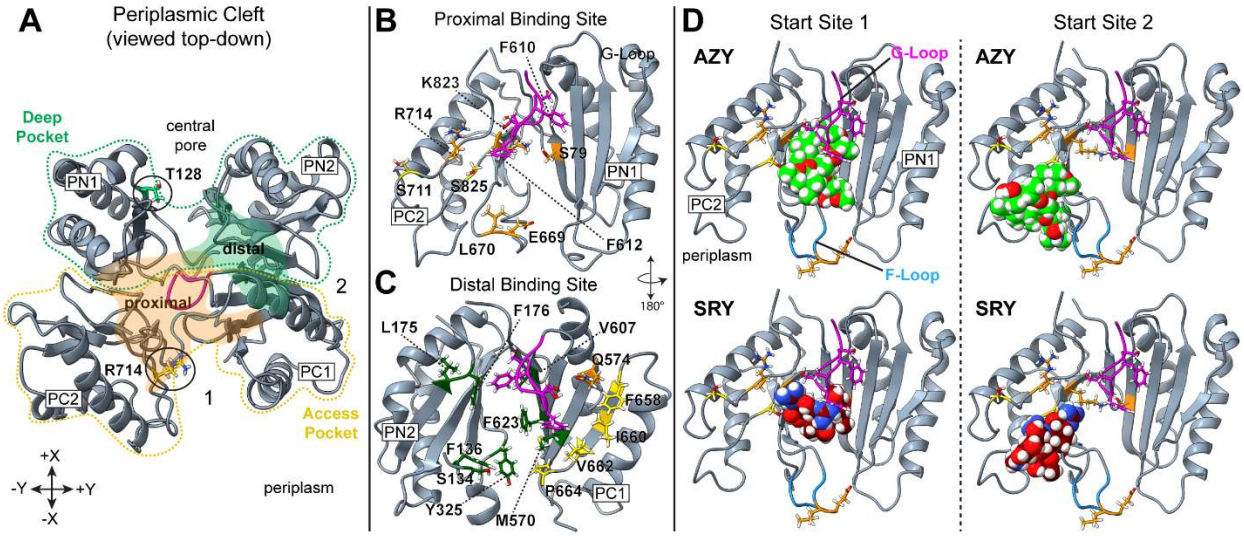

Fig 2. The Multidrug Binding Sites and Ligand Starting Sites within the Periplasmic Cleft of MtrD. A) The periplasmic cleft shown from the top down. The Deep Pocket (green) and Access Pocket (yellow) are outlined in dashed lines. The putative proximal and distal binding sites are shaded orange and green, respectively. The two possible entry pathways are numbered 1) the main entry path, and the 2) the alternate entry site that is only available to small substrates. **B)** The putative proximal binding site viewed from the side. Residues that may be important for substrate selectivity are shown in yellow sticks; residues of the proximal site that are conserved in AcrB are colored orange; the G-Loop is presented in magenta [13]. **C)** The putative distal binding site; residues that may be important for substrate selectivity are yellow sticks, proximal site residues that are conserved in AcrB are orange, distal site residues that are conserved in AcrB are dark green; G-Loop is magenta [13]. **D)** Ligand starting sites for TMD simulations, AZY in lime green, SRY in maroon.

In light of these characteristics of MtrD, and in order to generate reasonable starting positions of transport substrates in the TMD simulations, we independently docked AZY and SRY to the periplasmic cleft of MtrD using Autodock Vina [6, 28, 29]. For these experiments, docking search volumes sampled the entire conformational space within the periplasmic cleft (S2 Fig). The resultant docking sites of SRY and AZY are shown in Fig S3. Notably, the predicted docking poses for SRY and AZY clustered in the center of the periplasmic cleft near the G-Loop with outliers at the extremes of the Access or Deep Pockets, (S3 Fig). Our docking studies suggest that the periplasmic cleft in the Access conformation can accommodate multiple potential binding modes of AZY and SRY, despite their large sizes. We selected two poses from the resultant locations to serve as ligand "start sites" for the TMD simulations. In Site 1, SRY or AZY associates with the G-Loop and interacts with residues of the proximal binding site (Fig 2D,

bioRxiv preprint doi: https://doi.org/10.1101/2021.02.24.432727; this version posted February 24, 2021. The copyright holder for this preprint (which was not certified by peer review) is the author/funder. All rights reserved. No reuse allowed without permission.

left panel). In Site 2, SRY or AZY is bound near the entrance of the cleft and interacts with the foremost residues of the proximal binding site (Fig 2D, right panel).

Multiple protonation states of AZY are included in TMD simulations

The promiscuity of RND transporters contributes significantly to their effectiveness in conferring antibiotic resistance [8, 9, 13]. Since RND transporters often possess wide substrate profiles, one question to be asked is whether the substrate profile of MtrD extends to different protonation states of the same substrate. At physiological pH (between 7 and 7.5), three potential protonation states of AZY are possible: an uncharged form (AZY_{neu}); a singly protonated, positively charged form (AZY_{h1}); and a doubly protonated, positively charged form (AZY_{h2}) (S4 Fig) [30, 31]. In contrast, at physiological pH values, only one protonation state of SRY is likely to occur (S4 Fig). To investigate how each of these forms might interact with MtrD, we included each of the possible protonation states of AZY our TMD simulations (see Methods). Additionally, we note that the ionizable residues of MtrD are protonated (by default) according to a physiological pH of 7.4 in our MD simulations with both AMBER and NAMD. Histidines, the only residue that significantly ionizes at physiological pH of 7.4, default to protonation of the ε nitrogen in both NAMD and AMBER simulations [32, 33].

Defining "transport" in TMD simulations

Since large substrates are thought to travel from the Access Pocket to the Deep Pocket [6], it was of interest to quantify this movement, if any, during TMD simulations. We quantified ligand movement in two ways: first, we calculated the root mean squared deviation (RMSD) of the putative transport substrate from its starting position throughout the simulation. In our simulated system, the protein is oriented such that substrates, when moving in the transport direction away from the Access Pocket, move on a diagonal in the X-Y plane. Thus, $RMSD_{ligand}$ provides an approximation of ligand movement without necessitating quantification of movement along two axes. However, since RMSD calculations do not differentiate translational movement from rotational movements with little or no translational displacement, we also calculated the distance between the ligand's center of mass ($Ligand_{COM}$) and specific "checkpoint" residues

bioRxiv preprint doi: https://doi.org/10.1101/2021.02.24.432727; this version posted February 24, 2021. The copyright holder for this preprint (which was not certified by peer review) is the author/funder. All rights reserved. No reuse allowed without permission.

on the interior surface of the periplasmic cleft. For this secondary method of quantification, we chose the α-carbons of R714 in the entrance of the periplasmic cleft, and T128 at the exit of the cleft, as our "checkpoints" (Fig 2A). Both R714 and T128 were chosen solely based upon their positions and overall movement within the periplasmic cleft interior – both residues primarily move on an axis perpendicular to the direction of transport, and exhibit an overall RMSD of ~2.5 Å. If a ligand is transported, the $Ligand_{COM}$:$R714_{\alpha\text{-carbon}}$ distance should increase over time, and the $Ligand_{COM}$:$T128_{\alpha\text{-carbon}}$ distance should decrease over time (Fig 2A). In our simulations, we defined a ligand as "transported by MtrD" if, by the end-of-simulation, all three of the following conditions were met: the distance between the $Ligand_{COM}$ and $R714_{\alpha\text{-carbon}}$ was greater than or equal to 18 Å, the distance between the $Ligand_{COM}$ and $T128_{\alpha\text{-carbon}}$ was less than or equal to 15 Å, and the ligand RMSD was at least 8.5 Å.

Azithromycin is transported by MtrD in TMD simulations

Using known conformations of MtrD homologues as targets to mimic a putative efflux cycle of MtrD (S1 Fig), we performed 20 independent TMD simulations per protonation state of AZY at Site 1 and Site 2 (n = 20 TMD simulations per ligand, per start site). Based upon the previously defined distance cutoffs between $Ligand(s)_{COM}$ and $R714_{\alpha\text{-carbon}}$ or $T128_{\alpha\text{-carbon}}$, we divided the simulation outcomes into two clusters: Transported (Fig 3A-C) and Non-Transported substrates (S5 Fig). For each protonation state of AZY, we observed the following frequencies of transport: AZY_{neu} was transported in 12/20 simulations; AZY_{h1} was transported in 3/20 simulations; AZY_{h2} was transported in 6/20 simulations. Within the "Non-Transport" cluster of AZY trajectories, we observed two possible outcomes: 1) AZY remained in the same relative position straddling the G-Loop, or 2) AZY traveled into the Deep Pocket but remained closely associated with the G-Loop (S5 Fig). Examples of a both Transport and Non-Transport trajectories are shown in S1 Movie.

bioRxiv preprint doi: https://doi.org/10.1101/2021.02.24.432727; this version posted February 24, 2021. The copyright holder for this preprint (which was not certified by peer review) is the author/funder. All rights reserved. No reuse allowed without permission.

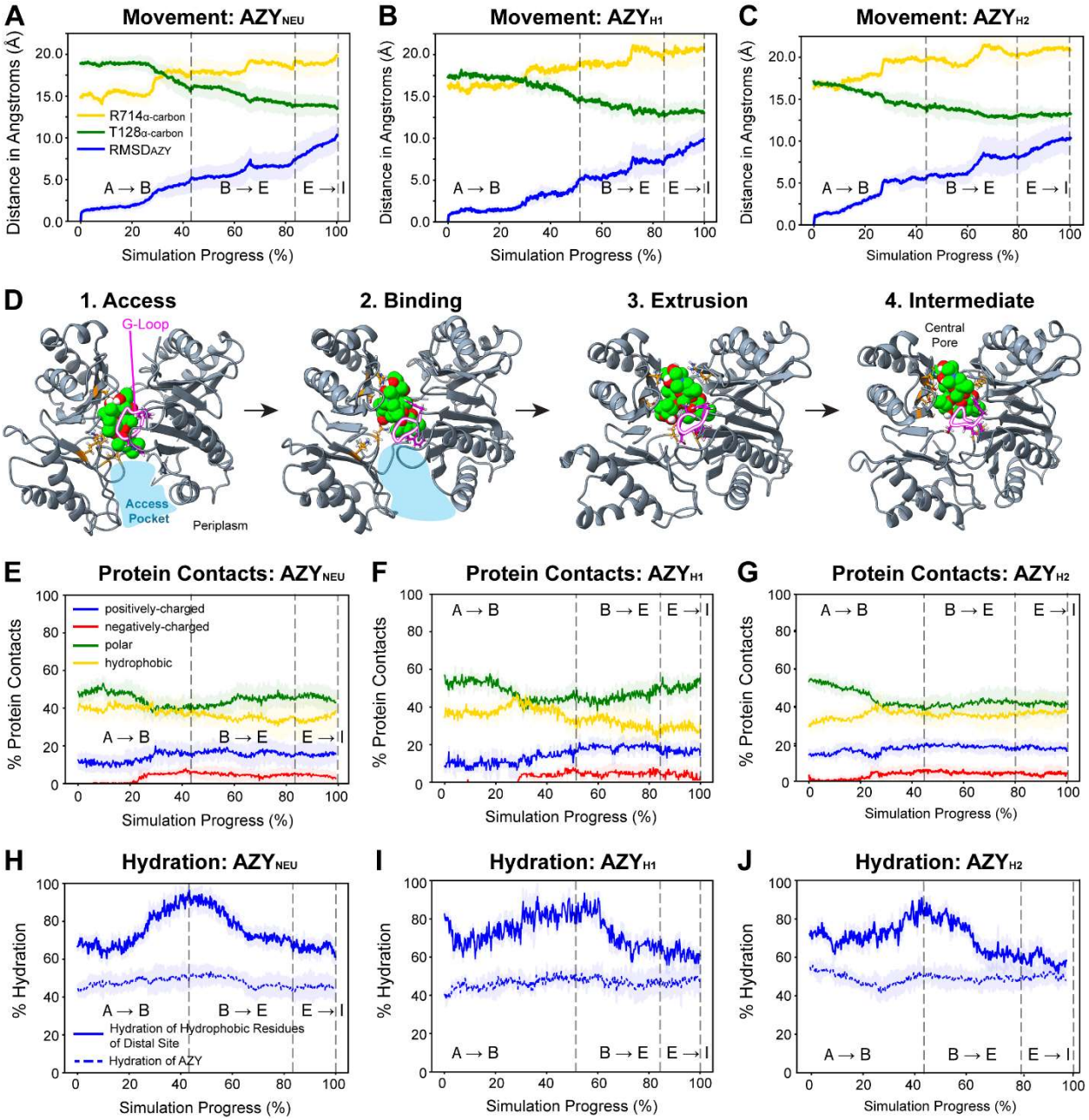

Fig 3. Transport of Azithromycin by MtrD in TMD Simulations. Panels A-C) show the RMSD of AZY from its starting position over time, and also the distance between the center of mass of AZY and the α-carbons of T128 or R714 in the periplasmic cleft. These movements were used to define 'Transport' or 'Non-Transport' of AZY in TMD simulations. **D)** is a representative trajectory that shows transport of AZY (lime green) through the periplasmic cleft, along with the accompanying conformational changes of a putative transport cycle. A transparent blue overlay shows the approximate size of the Access Pocket in the Access and Binding conformations, as the Access Pocket is closed in Extrusion and Intermediate. The G-Loop is outlined in magenta for visibility. **E-G)** show the chemical nature of protein-AZY contacts over the course of the simulation; the majority are either polar or hydrophobic. **H-J)** show the hydration of the solvent accessible surface area $(SASA)_{AZY}$, or of the hydrophobic residues in the putative distal binding site in the Deep Pocket, over the course of the simulation (see Methods). Data in **Panels A-C,** and **E-I)** represent the mean ± one standard deviation in shading. Dashed grey lines indicate when MtrD reaches a structural checkpoint. MtrD begins in the 'A' (Access), conformation, and transitions to the following: 'B' (Binding), 'E' (Extrusion), and 'I' (Intermediate); timepoints between the dashed lines indicate structural transitions between two states.

bioRxiv preprint doi: https://doi.org/10.1101/2021.02.24.432727; this version posted February 24, 2021. The copyright holder for this preprint (which was not certified by peer review) is the author/funder. All rights reserved. No reuse allowed without permission.

AZY travels farther when a fourth "intermediate" state is simulated

In addition to the known Access, Binding and Extrusion conformations, a fourth potential 'Resting' structure was identified in CmeB *Campylobacter jejuni*; CmeB shares a 28.7% sequence identity with MtrD [17] (Figs 1 E,F S1). The Resting conformation was classified by 1) the closure of the Access Pocket to the periplasm, and 2) the positioning of the transmembrane helices, which mimics that of the Extrusion conformation [17]. Su et al. observed that the Resting conformation occurred in the absence of a transport ligand and was most stable in the absence of a proton motive force (PMF) [17]. Because of this data, Su et al. postulated that this conformation could be a low-energy resting conformation of the transporter. It should be noted, however, that a proton gradient across the plasma membrane is present in actively reproducing Gram-negative bacterial cells [34]. Furthermore, in our TMD simulations, we found that the inclusion of this conformation as the last step of the TMD sequence resulted in the additional movement of AZY in the transport direction (Fig 3A-C, "E → I"). Consequently, we hypothesize that the Resting state likely participates in transport as a potential intermediate between Extrusion and Access, and may even serve to position particularly bulky substrates for disassociation. We refer to this conformation as an "Intermediate" structure, as it may be an intermediate conformation that occurs during the shift from Extrusion back to Access (Fig 3, abbreviated as "I").

An additional consideration for our TMD simulations is the relationship between conformational changes of the periplasmic cleft and the extrusion of a ligand into the funnel domain. Specifically, it is unclear whether (1) conformational changes of the periplasmic cleft squeeze the substrate into the funnel domain, or (2) the monomer adopts the Extrusion conformation, thereby maneuvering the ligand into a favorable position for disassociation, and then "waits" for the ligand to disassociate. Since forces were not applied to the ligands in our simulations, and the exact timing of substrate release is unknown, we were uncertain if we would observe disassociation of the ligand in our TMD simulations. Therefore, to prepare for the possibility that we may observe AZY release in our simulations, we modeled a full putative catalytic transport cycle, including this fourth putative Intermediate intermediary, but used it as the last step in our TMD cycle (S1 Fig).

bioRxiv preprint doi: https://doi.org/10.1101/2021.02.24.432727; this version posted February 24, 2021. The copyright holder for this preprint (which was not certified by peer review) is the author/funder. All rights reserved. No reuse allowed without permission.

In the TMD simulations performed here, we did not observe the movement of AZY in any protonation state into the funnel domain. This is not surprising, since an earlier MD computational study with the AcrB substrate Doxorubicin relied upon steered MD forces to pull Doxorubicin from the distal binding site, thereby necessitating dissociation [35]. However, as mentioned previously, with the inclusion of the putative Intermediate state in our target sequence, we observed that AZY traveled farther through the Deep Pocket (2.5 - 3 Å increase in distance traveled) and was thus in a better position for release/dissociation events to occur (Fig 3D, 'Intermediate').

Hydration of AZY mediates transport and outcompetes potential hydrophobic interactions

Large substrates, particularly macrolides like AZY, are thought to bind at the putative distal site (formed by PN2, PC1, and the G-Loop) when the monomer is in the Binding state, and protein-macrolide contacts are thought to be dominated by hydrophobic interactions (Fig 2C) [9, 13, 16, 35]. The cryo-EM structure of $MtrD_{CR103}$, an MtrD variant which confers elevated AZY resistance, contained erythromycin bound at the putative distal site. In this structure (PDB ID 6VKT, chain B), 71% of protein-erythromycin contacts were contributed by hydrophobic residues, and 21% and 7% by polar or positively charged residues, respectively [13]. Of these protein-erythromycin contacts, 43% were contributed by PN2, 43% by PC1, and 14% by the G-Loop; additionally, the residues involved are conserved in both wild-type MtrD and $MtrD_{CR103}$. Therefore, when MtrD was approaching or in the Binding conformation in our simulations, we expected that AZY would interact closely with the putative distal binding site and primarily with PN2, PC1 and the G-Loop. As expected, when AZY was transported, we found that the G-Loop accounted for a significant share (21-30%) of protein-AZY contacts at the Binding conformation (Table 1). However, we observed that most of the protein-AZY contacts (39-43% at Binding) were contributed by PN1, whose role in substrate extrusion has not been previously studied, and that PN2 and PC1 contributed only a small fraction of contacts, 6 to 15% and 0.6 to 7%, respectively. (Table 1).

bioRxiv preprint doi: https://doi.org/10.1101/2021.02.24.432727; this version posted February 24, 2021. The copyright holder for this preprint (which was not certified by peer review) is the author/funder. All rights reserved. No reuse allowed without permission.

Transport Cluster		Percent (%) of Protein-Ligand Contacts Contributed by Domain or Region							
	Structure	**G-Loop**	**PC1**	**PC2**	**PN1**	**PN2**	**F-Loop**	**AP**	**DP**
AZY_{neu}	Access	17.0 ± 2.5	13.0 ± 4.0	38.0 ± 4.1	29.3 ± 4.4	0.4 ± 0.4	2.3 ± 1.0	51.0 ± 3.1	29.7 ± 4.6
	Binding	27.0 ± 4.3	2.4 ± 2.1	9.8 ± 8.3	39.8 ± 8.7	5.9 ± 4.6	15.1 ± 6.0	12.2 ± 7.7	45.7 ± 10.0
	Extrusion	21.8 ± 3.0	3.4 ± 3.5	4.9 ± 3.7	47.1 ± 6.6	15.5 ± 8.1	7.4 ± 5.6	8.3 ± 2.9	62.6 ± 8.5
	Intermediate	18.6 ± 3.3	2.6 ± 2.8	4.1 ± 4.0	46.9 ± 7.0	22.8 ± 9.4	5.0 ± 4.1	6.6 ± 3.5	69.7 ± 7.2
AZY_{h1}	Access	16.8 ± 2.2	13.3 ± 1.6	19.7 ± 1.2	41.1 ± 2.6	2.6 ± 0.3	6.4 ± 0.4	33.0 ± 2.5	43.8 ± 2.4
	Binding	29.9 ± 4.2	7.0 ± 5.0	1.8 ± 1.9	43.7 ± 4.3	8.4 ± 3.4	9.2 ± 8.8	8.8 ± 5.7	52.1 ± 1.8
	Extrusion	27.3 ± 3.7	5.7 ± 3.5	1.8 ± 1.3	41.7 ± 5.5	16.0 ± 5.9	7.5 ± 7.6	7.4 ± 4.2	57.7 ± 11.3
	Intermediate	25.2 ± 1.7	6.0 ± 3.3	1.8 ± 1.5	44.0 ± 7.0	19.2 ± 5.3	3.7 ± 3.3	7.9 ± 4.8	63.2 ± 5.2
AZY_{h2}	Access	19.6 ± 2.5	0.6 ± 1.0	30.2 ± 2.0	44.2 ± 4.0	2.4 ± 1.2	3.1 ± 1.4	30.7 ± 2.3	46.6 ± 4.0
	Binding	21.0 ± 3.5	0.6 ± 1.3	8.6 ± 4.1	42.9 ± 5.4	16.0 ± 6.5	10.8 ± 8.5	9.2 ± 4.1	58.9 ± 9.6
	Extrusion	19.8 ± 5.2	0.0 ± 0.0	1.9 ± 3.0	43.4 ± 4.1	31.9 ± 7.5	3.1 ± 4.5	1.9 ± 3.0	75.3 ± 8.4
	Intermediate	22.6 ± 2.4	0.1 ± 0.3	2.3 ± 2.6	41.6 ± 6.0	31.3 ± 7.7	1.9 ± 2.6	2.5 ± 2.7	72.9 ± 5.9
Non-Transport Cluster		**Percent (%) of Protein-Ligand Contacts Contributed by Domain or Region**							
	Structure	**G-Loop**	**PC1**	**PC2**	**PN1**	**PN2**	**F-Loop**	**AP**	**DP**
AZY_{neu}	Access	18.2 ± 2.9	14.4 ± 2.4	38.3 ± 2.7	26.2 ± 3.9	0.1 ± 0.3	2.8 ± 1.0	52.7 ± 3.7	26.3 ± 3.8
	Binding	24.3 ± 6.7	3.7 ± 4.9	25.0 ± 9.4	25.8± 11.0	0.0 ± 0.0	21.2 ± 4.7	28.6 ± 9.1	25.8 ± 11.0
	Extrusion	18.1 ± 4.8	6.0 ± 4.7	21.0 ± 8.7	32.2 ± 5.4	6.8 ± 6.5	15.9 ± 5.0	27.1 ± 9.0	39.0 ± 10.2
	Intermediate	17.9 ± 2.4	5.1 ± 3.8	21.1 ± 7.1	35.1 ± 4.5	7.5 ± 6.5	13.3 ± 3.1	26.2 ± 8.1	42.6 ± 8.5
AZY_{h1}	Access	16.3 ± 1.7	14.4 ± 30	19.6 ± 1.3	40.2 ± 3.0	2.1 ± 0.5	7.4 ± 0.9	34.0 ± 2.9	42.2 ± 3.2
	Binding	26.8 ± 5.4	2.6 ± 2.3	12.0 ± 6.7	37.4 ± 9.7	4.2 ± 4.5	17.0 ± 5.0	14.6 ± 6.6	41.6 ± 10.8
	Extrusion	23.4 ± 3.7	3.6 ± 4.0	11.6 ± 8.2	37.0 ± 6.2	10.5 ± 7.5	14.0 ± 4.1	15.2 ± 9.6	47.4 ± 11.7
	Intermediate	21.8 ± 2.4	3.2 ± 3.1	12.7 ± 7.6	36.5 ± 4.9	13.1 ± 6.9	12.6 ± 5.3	15.9 ± 8.2	49.7 ± 10.3
AZY_{h2}	Access	19.8 ± 1.5	0.3 ± 0.6	29.9 ± 2.7	43.2 ± 4.1	3.4 ± 1.6	3.2 ± 1.3	30.3 ± 2.9	46.7 ± 3.5
	Binding	25.3 ± 9.1	0.2 ± 0.7	15.0 ± 6.1	45.0± 11.5	5.4 ± 5.2	9.2 ± 5.3	15.2 ± 6.0	50.3 ± 10.5
	Extrusion	20.8 ± 6.3	0.0 ± 0.0	10.8 ± 3.1	43.5 ± 7.2	16.8 ± 5.6	8.0 ± 4.9	10.8 ± 3.1	60.4 ± 6.6
	Intermediate	18.4 ± 3.3	0.2 ± 0.9	12.8 ± 4.7	45.3 ± 4.0	16.2 ± 5.6	7.1 ± 4.4	13.0 ± 4.7	61.5 ± 6.4

Table 1. Percentage of Protein-AZY Contacts Contributed by Specific Domains of the MtrD Periplasmic Cleft. Contacts are defined as residues whose α-carbon is within 4 Å of AZY at each timepoint of the simulation. Individual domains of the periplasmic cleft are as defined in [13], and the % protein contacts for the Access Pocket (PC1&PC2) and Deep Pocket (PN1&PN2) have also been calculated from the mean contact value. Contact analysis was performed for trajectories in the "Transport" cluster using VMD and analyzed with scripts in *Tcl* and python.

Based upon the structure of erythromycin-bound $MtrD_{CR103}$, we also expected that the majority (~ 70%) of protein-AZY contacts at Binding would be contributed by hydrophobic residues; instead, we found that polar and hydrophobic residues each contributed ~40% of contacts (except for AZY_{h1}, where polar contacts outnumbered hydrophobic contacts) (Fig 3E-G). At Binding, this difference from the expected value can be attributed to the share of contacts contributed by PN1, which are mostly polar in nature, and the lack of (expected) contacts with the hydrophobic patch formed by PC1 and PN2. Here it is helpful to

bioRxiv preprint doi: https://doi.org/10.1101/2021.02.24.432727; this version posted February 24, 2021. The copyright holder for this preprint (which was not certified by peer review) is the author/funder. All rights reserved. No reuse allowed without permission.

note that, for the purposes of this work, "contacts" are defined as residues of MtrD within 4 Å of any atom of AZY at a particular point in the simulation. The diameter of a water molecule is ~2.8 Å [36]. Thus, it is possible for a hydrophobic residue to be counted as a "contact" with AZY, but to also be separated from AZY by a layer of water, which would prevent a true hydrophobic interaction from occurring via the occlusion of water molecules between AZY and the residue of interest. To elucidate the nature of protein-AZY contacts, we calculated the percent hydration of the potential solvent accessible surface area (SASA) of AZY (in all protonation states) and of the hydrophobic residues of the putative distal site (formed by PC1/PN2) over the course of the TMD simulations (Fig 3H-J).

When AZY was transported, we observed that the $SASA_{AZY}$ was ≥ 45% hydrated throughout transport. Notably, the SASA of the hydrophobic residues in the distal site ($SASA_{distal\ hydrophobic}$) was ≥ 60% hydrated throughout the entire simulation. During the Binding conformation, when the association between AZY and these hydrophobic residues is thought to occur, the $SASA_{distal\ hydrophobic}$ of the increases to 80-90% (Fig 3H-J). Furthermore, the ligand is associating primarily with PC2/PN1 and the G-Loop, not with PC1/PN2 (Table 1). These data suggest that significant hydrophobic interactions between the hydrophobic residues of the distal site and AZY are unlikely to occur at the Binding stage of our TMD simulations. However, the hydration of $SASA_{AZY}$ and $SASA_{distal}$ exhibited similar trends between the Transport and Non-Transport clusters (S5 Fig). Furthermore, instead of the expected domination of hydrophobic interactions with the putative distal site and PN2, the majority of protein-AZY contacts were contributed by PN1, which has not previously been suggested to contribute to substrate recognition or extrusion. The second largest share of contacts was contributed by hydrophobic residues of the G-Loop, which is thought to filter and orient potential substrates throughout the transport process.

While our data support the hypothesis that water plays a role in mediating substrate movement through the periplasmic cleft [35], the data also suggest that something other than water is causing AZY to travel farther in the Transport cluster. As mentioned previously, the closing of the periplasmic cleft during Extrusion or the putative Intermediate states causes AZY to move farther towards the funnel domain. Not only does this conformational transition restrict access to the entrance of the periplasmic cleft, but it also significantly restricts the available space within the cleft. This is particularly apparent in the case of the

bioRxiv preprint doi: https://doi.org/10.1101/2021.02.24.432727; this version posted February 24, 2021. The copyright holder for this preprint (which was not certified by peer review) is the author/funder. All rights reserved. No reuse allowed without permission.

Intermediate (aka "Resting") structure, in which the periplasmic cleft channel is almost entirely closed, except for an area quite close to the exit of the cleft [17]. We hypothesize that the transport of AZY by MtrD is mediated through a combination of 1) protein-ligand interactions, 2) gated access to specific areas of the periplasmic cleft, 3) a peristaltic-like squeezing caused by the cycle of conformational changes, and 4) hydration of the substrate.

Streptomycin was not transported by MtrD in TMD simulations.

In TMD simulations with SRY started at Site 1, using the same simulation routines and transport criteria as for AZY, SRY was classified as 'not transported' in 20 out of 20 trajectories (Fig 4). The mean $RMSD_{SRY}$ was 6.2 ± 1.7 Å (Fig 4A). The starting position of SRY at Site 1 is shown in Fig 4B, and the ending positions of SRY in all trajectories, as well as representative TMD simulations, are shown in Fig 4C and S2 Movie. As shown in Fig 4C, SRY remains closely associated with the G-Loop, particularly F612 and S613, throughout the TMD simulations. While hydrogen bonding between SRY and S91 is predicted to occur in our post-simulation analyses, over 75% of the available SASA of SRY, including the guanidinium group that contacts S91, was hydrated throughout all of our TMD simulations (Fig 4D). Furthermore, we found that polar contacts from PN1 and PC2 dominate the protein-SRY interactions throughout the entire conformational cycle of MtrD, followed by hydrophobic interactions with the G-Loop (Fig 4C,E and Table 2). SRY did not interact significantly with the PC1 or PN2 domains (Table 2). In these simulations, we observed that SRY displayed significantly more conformational flexibility than AZY. Our results indicate that SRY, if placed in the proximal binding site at Site 1, does not exhibit transport behavior in these simulations.

bioRxiv preprint doi: https://doi.org/10.1101/2021.02.24.432727; this version posted February 24, 2021. The copyright holder for this preprint (which was not certified by peer review) is the author/funder. All rights reserved. No reuse allowed without permission.

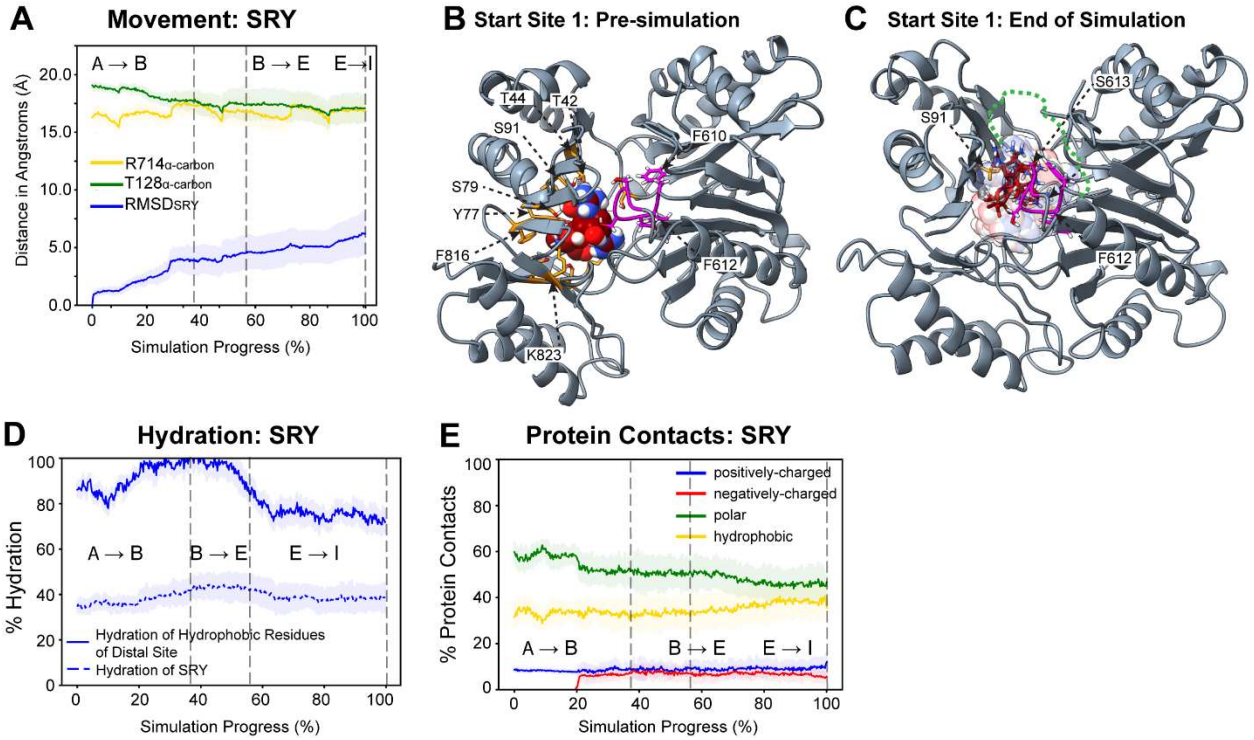

Fig 4. Interactions of Streptomycin with the Periplasmic Cleft at Site 1. Panel A) shows the RMSD of SRY from its starting position over time, and the distance between the center of mass of SRY and the α-carbons of T128 or R714 in the periplasmic cleft. **B)** shows SRY at Site 1 in the Access Pocket at the beginning of the TMD Simulations. **C)** shows all endpoints of SRY superimposed; one ending position of SRY, the position closest to fulfilling the criteria for "Transport", is shown in opaque licorice representation; the other "non-transport" ending positions are in semi-transparent spacefill representation. A green dashed line marks the ending position of AZY in a transport trajectory as a reference. **D)** shows the percent (%) hydration of the $SASA_{SRY}$ over the course of the simulation. **E)** shows the nature of protein-SRY contacts formed throughout the simulation. In **B)** and **C)**, labeled residues in orange sticks interact with SRY in at least 80% of the TMD simulations with the G-Loop in magenta.

SRY	Percent (%) of Protein-Ligand Contacts Contributed by Domain or Region							
Structure	**G-Loop**	**PC1**	**PC2**	**PN1**	**PN2**	**F-Loop**	**AP**	**DP**
Access	6.0 ± 0.1	0.0 ± 0.0	49.1 ± 1.5	45.0 ± 1.6	0.0 ± 0.0	0.0 ± 0.0	49.1 ± 1.5	45.0 ± 1.2
Binding	11.1 ± 3.0	0.0 ± 0.0	39.8 ± 0.4	47.1 ± 1.4	0.1 ± 0.0	2.0 ± 2.0	39.8 ± 0.4	47.1 ± 1.4
Extrusion	21.3 ± 1.1	0.0 ± 0.0	31.7 ± 4.8	34.1 ± 0.3	0.1 ± 0.0	13.0 ± 3.5	31.7 ± 4.8	34.1 ± 0.3
Intermediate	22.5 ± 8.8	0.0 ± 0.0	15.8 ± 6.7	49.3 ± 4.3	1.3 ± 1.3	11.2 ± 5.1	15.8 ± 6.7	50.5 ± 3.0

Table 2. Percentage of Protein-SRY Contacts Contributed by Specific Domains of the MtrD Periplasmic Cleft. Contacts are defined as residues whose α-carbon is within 4 Å of SRY at each timepoint of the simulation. Individual domains of the periplasmic cleft are as defined in [13], and the % protein contacts for the Access Pocket (PC1 and PC2) and Deep Pocket (PN1 and PN2) have also been calculated from the mean contact value. Contact analysis was performed for trajectories in the "Transport" cluster using VMD and analyzed with scripts in *Tcl* and python.

bioRxiv preprint doi: https://doi.org/10.1101/2021.02.24.432727; this version posted February 24, 2021. The copyright holder for this preprint (which was not certified by peer review) is the author/funder. All rights reserved. No reuse allowed without permission.

Azithromycin exhibits variable behavior at the periplasmic cleft entrance

AZY is a known substrate of MtrD [3, 10, 30, 37]. Due to its large size and the timescale of our TMD simulations, we did not expect to see AZY diffuse from the periplasmic cleft entrance towards the G-Loop. Indeed, if the initial process of G-Loop association is a passive diffusional process, as is suggested by available crystal structures, we would not expect to observe AZY interaction with the G-loop here. Consistent with these expectations, when AZY was placed at the very entrance of the periplasmic cleft, it largely remained within the cleft created by PC1/PC2 for the duration of the subsequent TMD simulations. In 2/20 simulations, AZY_{neu} slipped from the periplasmic cleft into the periplasmic space but remained closely associated with the outer surfaces of the periplasmic cleft. This occurred in 1/20 simulations for AZY_{h1}, and 1/20 for AZY_{h2} and is unsurprising given the timescale of the simulations and the fact that the periplasmic cleft closed without AZY being near the G-Loop or farther back in the pocket. In combination with our data from Site 1, these simulations suggest that the initial process of substrate capture and subsequent movement towards the G-Loop, is likely a slow process governed by diffusion. The full results of our TMD simulations with AZY at Start Site 2, and all resultant positions of AZY, are shown in S6 Fig and in S3 Movie [5].

Although we did not see the diffusion of AZY towards the G-Loop from Site 2 in our TMD simulations, we unexpectedly observed close interactions between AZY_{h1} and the TM9 linker (S3 Movie). These interactions were also observed with AZY_{h2}, but not with AZY_{neu}. The uppermost portion of TM9 and its linker (residues 917-927) is thought to be unique to MtrD, projects away from the "body" of the MtrD homotrimer, and out of the membrane into the periplasm [6, 38]. In addition to substrate capture from the periplasm, it has been suggested that RND transporters can capture substrates from the inner membrane-periplasm interface [39]. Both AZY_{h1} and AZY_{h2} are weakly positively charged, and since gram negative inner membranes contain negatively-charged POPG lipids, it is possible that these AZY species associate with the periplasmic leaflet of the inner membrane prior to capture by MtrD [40]. Since TM9 projects out from the entrance to the periplasmic cleft, a bulky substrate would presumably contact TM9 prior to entering the periplasmic cleft. We also note that bulky substrates cannot enter directly through the uppermost regions of the cleft entrance, due to the presence of the membrane fusion protein MtrC (S7 Fig)

bioRxiv preprint doi: https://doi.org/10.1101/2021.02.24.432727; this version posted February 24, 2021. The copyright holder for this preprint (which was not certified by peer review) is the author/funder. All rights reserved. No reuse allowed without permission.

[41]. Therefore, it is possible that the uppermost region of TM9, which is composed of mostly polar or charged residues, could assist in capture of charged, amphiphilic substrates of MtrD. The role of this unique region of TM9 in substrate capture warrants further study.

Streptomycin is rejected from the periplasmic cleft entrance

Since SRY is not a recognized substrate of MtrD, we acknowledged that the positioning of SRY within the periplasmic cleft at Site 1 (Figs 2D, 5A) may be unlikely to occur naturally [7]. To test this assumption, we examined our simulation results from Start Site 2 to see whether SRY could diffuse past the putative selectivity filter formed by residues at the periplasmic cleft entrance (Fig 2C-D). In contrast to the behavior of AZY in any simulation performed by us, we observed SRY moving 'backwards', i.e. away from the interior of the periplasmic cleft. In 20/20 subsequent TMD simulations, SRY dissociated from the interior of the periplasmic cleft and moved further into the solvent (periplasmic side), but remained closely associated with the solvent-exposed surfaces of the Access Pocket (S6 Fig). In the initial position at Site 2, SRY was found to be in close contact with two positively charged residues – R714 and K823 – both of which are thought to be important for macrolide recognition [13]. Since SRY is strongly positively charged, it is possible that a combination of 1) repulsive interactions with R714 and K823, and 2) unfavorable contacts with the mostly hydrophobic PC1 domain, contributed to the passive rejection of SRY from the periplasmic cleft. Once SRY exited the periplasmic cleft, the most frequent residue contact occurred in 14/20 trajectories with D709 (>70% of the simulation time) on the exterior surface of the periplasmic cleft. The results of TMD simulations of SRY at the cleft entrance are shown in S4 Movie.

The molecular landscape of the periplasmic cleft changes dynamically

As a member of Hydrophobic-Amphiphile family of RND transporters, MtrD transports a variety of structurally diverse hydrophobic or amphipathic molecules [9]. To investigate how the dynamic molecular landscape of the periplasmic cleft might facilitate substrate capture and diffusion, we performed analyses of the Molecular Lipophilicity Potential (MLP) and the Electrostatic Potential (EP) isosurfaces of the periplasmic cleft in the presence and absence of AZY.

bioRxiv preprint doi: https://doi.org/10.1101/2021.02.24.432727; this version posted February 24, 2021. The copyright holder for this preprint (which was not certified by peer review) is the author/funder. All rights reserved. No reuse allowed without permission.

Molecular lipophilicity potential (MLP) of the periplasmic cleft

MLP describes the 3D distribution of lipophilicity (i.e., affinity for polar or non-polar solvents) at a point in space or across a molecular surface, and is calculated by summing the lipophilic contributions of molecular fragments upon the surrounding environment [42]. A positive (+) MLP value indicates a *lipo*philic region (Fig 5, gold regions), and a negative (-) MLP indicates a *hydro*philic region (Fig 5, teal regions). Since the MLP describes lipophilicity in 3D, the MLP of a molecular surface is sensitive to changes in the structure of that surface. It is thought that ligand-receptor interactions may involve the interaction of complementary MLP patches (i.e. hydrophobic-hydrophobic), whereas mosaic MLP isosurfaces may contribute to weak, dispersive binding forces that might facilitate substrate transport [21, 42]. The first image of Fig 5A, which shows one half of the periplasmic cleft in the Access conformation, is an example of a mosaic-like MLP surface, where MLP of the available surface area is a patchwork of MLP-neutral or less-lipophilic surfaces. The second image of Fig 5A, showing the other half of the periplasmic cleft, shows an example of a large patch of surface area with a strongly lipophilic MLP.

bioRxiv preprint doi: https://doi.org/10.1101/2021.02.24.432727; this version posted February 24, 2021. The copyright holder for this preprint (which was not certified by peer review) is the author/funder. All rights reserved. No reuse allowed without permission.

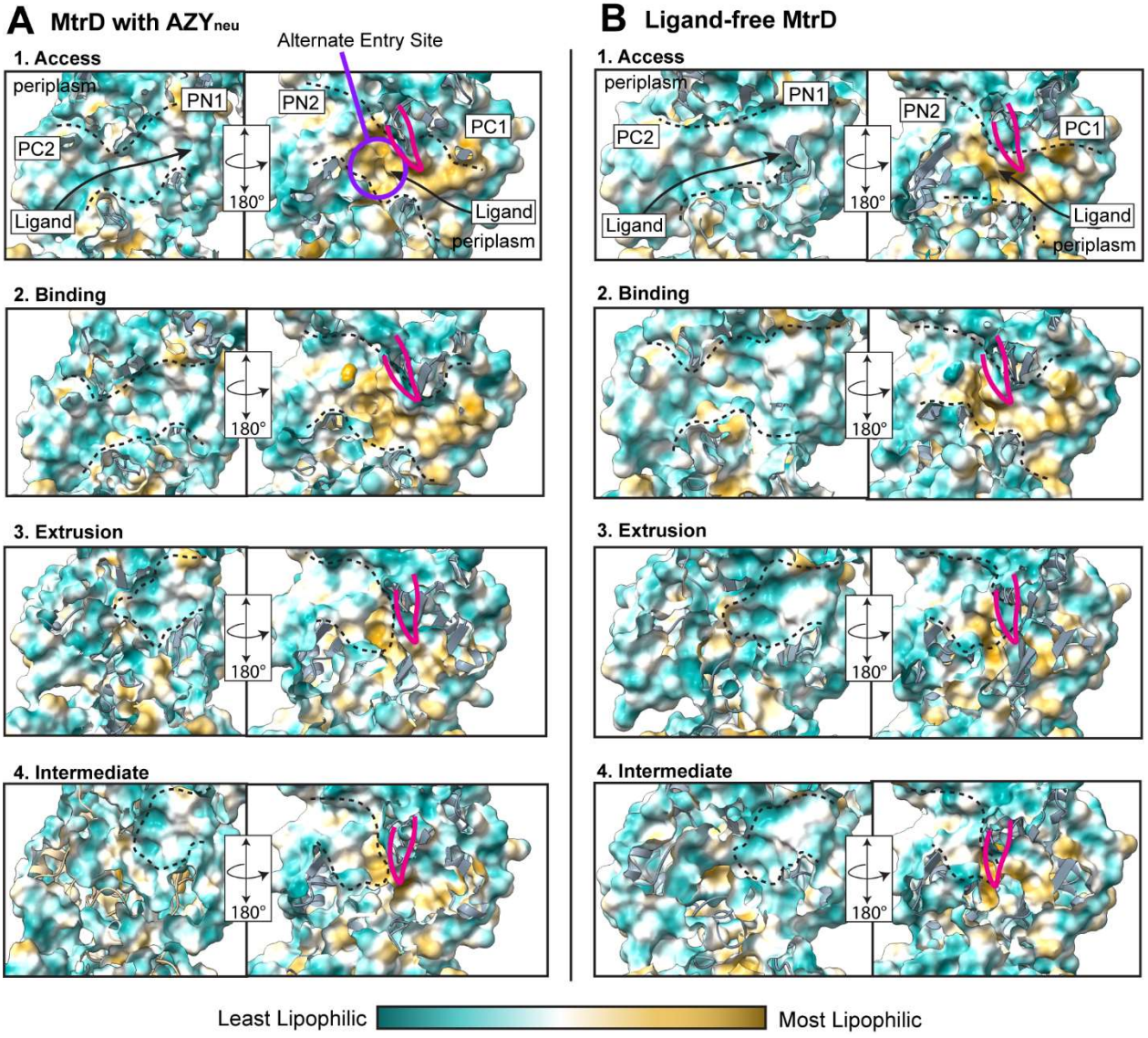

Fig 5. The Molecular Lipophilicity Potential Surfaces of the Periplasmic Cleft Change Dynamically during the Conformational Transitions of the Transport Process. Panels show the Molecular Lipophilicity Potential (MLP) surfaces plotted on the molecular surface representation of the periplasmic cleft **A)** in the presence of AZY_{neu} and **B)** in the absence of a Ligand. For visual aids, the channels formed by the periplasmic cleft at each conformation are approximated with dashed lines, the G-Loop is marked in magenta, and the direction of substrate travel is marked with a black arrow. MLP is colored teal to gold, from least lipophilic to most lipophilic. MLP was calculated using ChimeraX.

Through analysis of the AZY-bound or ligand-free monomer, we found that the available MLP isosurfaces of the periplasmic cleft change dynamically throughout the transport cycle. Fig 5A shows the MLP surfaces of AZY_{neu}-bound MtrD, and Fig 5B shows the surfaces of ligand-free MtrD in the same conformation. In Access, the MLP of PC2/PN1 was found to be a mosaic of polar-neutral areas, whereas the MLP of PN2/PC1 was much more lipophilic, particularly at the entrance of the periplasmic cleft and at

bioRxiv preprint doi: https://doi.org/10.1101/2021.02.24.432727; this version posted February 24, 2021. The copyright holder for this preprint (which was not certified by peer review) is the author/funder. All rights reserved. No reuse allowed without permission.

the alternate entry site for small, hydrophobic substrates (Fig 5A-B, Access). As a member of the hydrophobic-amphiphile (HAE) family of RND transporters, it is unsurprising that these two areas of the periplasmic cleft, both of which are thought to contribute to substrate filtration and capture, contain primarily lipophilic or weakly polar MLP isosurfaces.

In the Binding conformation, the division of the available surfaces within the periplasmic cleft is still apparent, with PC2/PN1 creating a mosaic of hydrophilic and neutral surfaces, and PN2/PC1 creating a 'lipophilic highway' that, at first glance, seems to extend directly through the cleft (Fig 5A-B, Binding). However, access to this 'lipophilic highway' is both obstructed and restricted by the G-Loop, i.e. to associate with the lipophilic areas of the Deep Pocket, bulky substrates must first contend with the G-Loop [9]. Our docking studies suggest that the G-Loop sterically hinders AZY from maintaining consistent contact with the PC1/PN2 domains during the transition from the Access Pocket to the Deep Pocket (S3 Fig). Instead, as shown in S3 Fig, the predicted binding modes of AZY in the periplasmic cleft follow a pathway that curves to the left side of the G-Loop; along this path, AZY would primarily contact PC2 and PN1. PC2 and PN1 are a mosaic of hydrophilic and neutral MLP isosurfaces (Fig 5, Binding), and as such, are particularly suited to facilitating the diffusion of an amphiphilic or hydrophobic substrate

In the Extrusion conformation, access to the PC1 and PC2 domains is restricted by A), the closure of the periplasmic cleft, and B) conformational shifts of the G-Loop. These changes prevent 'backflow' of the substrate into the Access Pocket. In the putative Intermediate conformation, there is even less available surface area to a ligand in the Deep Pocket, and the Access Pocket is still closed to the periplasm. In both the Extrusion and Intermediate conformations, the majority of available MLP isosurfaces (to a bound ligand) were found to be hydrophilic or neutral, apart from the hydrophobic stop-gap formed by the G-Loop (Fig 5A-B, Extrusion, Intermediate). These isosurfaces may serve to encourage substrates to leave the periplasmic cleft, as many MtrD substrates are hydrophobic or amphiphilic. Interestingly, analysis of the AZY-bound monomer reveals that the presence of AZY only slightly changed the MLP signatures of the periplasmic cleft (Fig 5B).

Through MLP analysis of the periplasmic cleft, we found that both substrate entry points contain significantly hydro*phobic* isosurfaces, and the only known exit consisted of primarily hydro*philic*-neutral

bioRxiv preprint doi: https://doi.org/10.1101/2021.02.24.432727; this version posted February 24, 2021. The copyright holder for this preprint (which was not certified by peer review) is the author/funder. All rights reserved. No reuse allowed without permission.

isosurfaces. Therefore, it appeared that substrates first interacted with complementary isosurfaces, and were subsequently shuttled to uncomplimentary or neutral isosurfaces deeper within the periplasmic cleft. Once the substrate reaches the Deep Pocket behind the G-Loop, the closure of the periplasmic cleft, and the shifting of the PC1/PN2 domains, restricts access to hydrophobic areas within the cleft. It appears to us therefore, that throughout the substrate transport cycle, transport ligand access to hydrophobic areas of the pump was alternately opened and restricted.

Electrostatic potential (EP) isosurfaces of the periplasmic cleft

As with MLP, the electrostatic potential (EP) isosurfaces of the periplasmic cleft change dynamically throughout the transport process. However, in contrast to the results of the MLP analyses, we observed that the EP isosurfaces changed significantly in the presence AZY. Fig 6A shows the EP of AZY_{neu}-bound MtrD, and panel B shows the EP of ligand-free MtrD. In the absence of AZY, the periplasmic cleft contained mildly negative or neutral isosurfaces (Fig 6B). In the presence of AZY, the cleft gained positive-neutral mosaic isosurfaces in the Access conformation and lost a significantly negative patch in the Binding conformation (Fig 6A). Furthermore, in the Extrusion and Intermediate conformations, a strongly positive region near the G-Loop was contributed by K823 (Fig 6A, Extrusion). Since forces were only applied to the α-carbons of the protein backbone in these simulations, the side chains and ligand were allowed to move freely. Therefore, changes in the EP isosurfaces are due presumably to (1) changes in the orientation of side chains and (2) the presence of AZY. Since AZY_{h1} and AZY_{h2} are weakly positively charged, it is possible that the strongly positive patch near the G-Loop serves to repel AZY away from the center of the cleft and up into the funnel domain of the transporter.

bioRxiv preprint doi: https://doi.org/10.1101/2021.02.24.432727; this version posted February 24, 2021. The copyright holder for this preprint (which was not certified by peer review) is the author/funder. All rights reserved. No reuse allowed without permission.

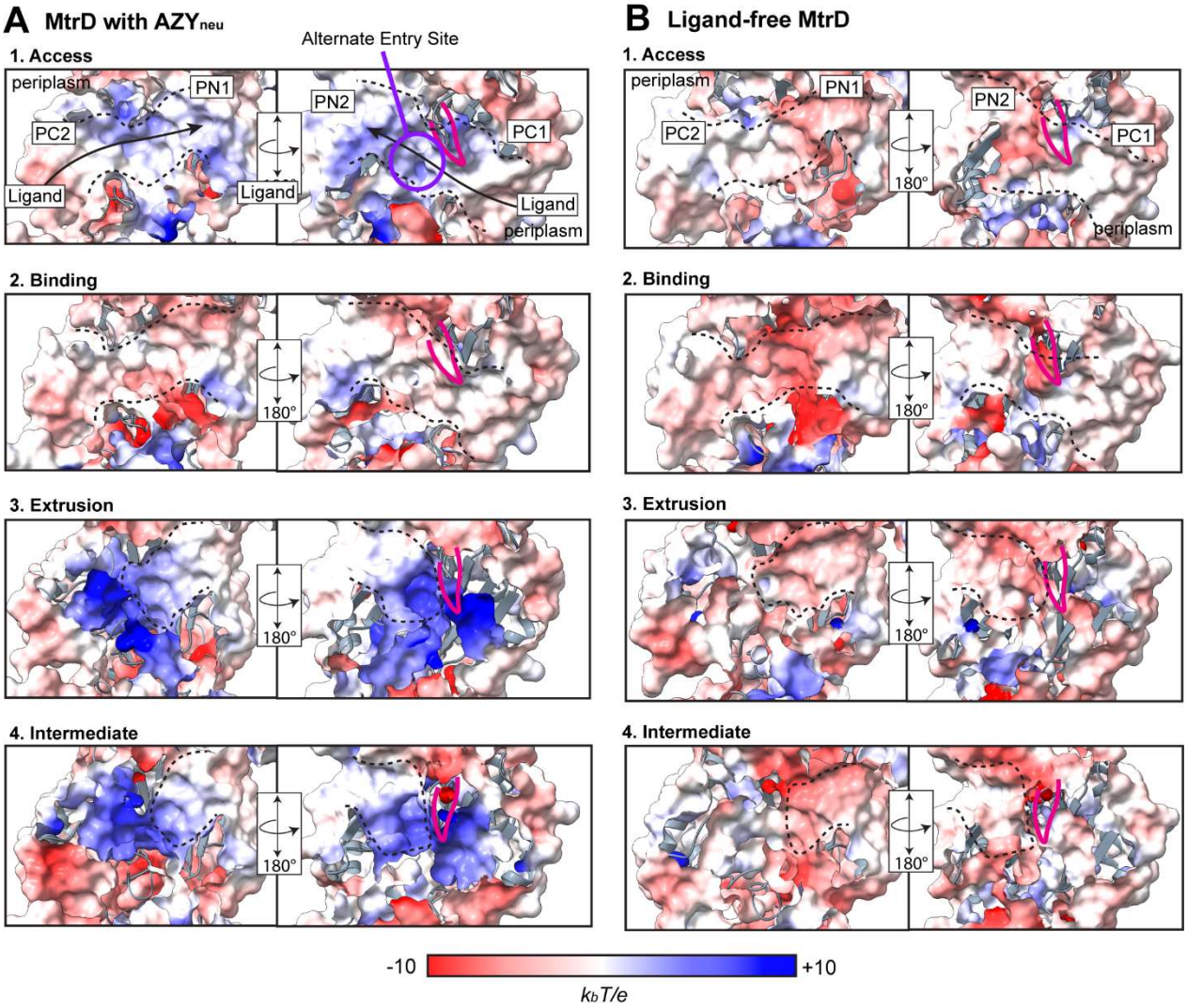

Fig 6. The Electrostatic Potential Surfaces of the Periplasmic Cleft Change Dynamically in the Presence of AZY. Panels show the Electrostatic Potential surfaces plotted on the molecular surface representation of the periplasmic cleft **A)** in the presence of AZY_{neu} and **B)** in the absence of a Ligand. For visual aids, the channels formed by the periplasmic cleft at each conformation are approximated with dashed lines, the G-Loop is marked in magenta, and the direction of substrate travel is marked with a black arrow. EP is colored red to blue, from negative (-10 k_bT/e) to positive (+10 k_bT/e) potential, where k_b is the Boltzmann constant, T is the absolute temperature (310K), and e is the electron charge. EP surfaces were calculated using the APBS online server and visualized with ChimeraX.

A potential role for MtrC in substrate recognition

Regarding the interpretation of our MD results, a significant consideration is the lack of the membrane fusion protein (or 'periplasmic adaptor') MtrC in our simulations. The complete MtrCDE complex assembles with a 3:6:3 stoichiometry; MtrC assembles as a hexamer, whilst MtrD and MtrE both assemble as trimers [43]. Since the structure of MtrC remains unsolved, we built a homology model using

bioRxiv preprint doi: https://doi.org/10.1101/2021.02.24.432727; this version posted February 24, 2021. The copyright holder for this preprint (which was not certified by peer review) is the author/funder. All rights reserved. No reuse allowed without permission.

AcrA from the AcrAB-TolC complex; AcrA shares a 44.6% sequence identity with MtrC (PDB ID 5NG5) [41]. A full model of MtrCDE was subsequently built using the structures of MtrD (4MT1), MtrE (4MTO), and the model of MtrC [6, 44]. To assemble MtrCDE, the fully-assembled AcrAB-TolC (5NG5) was used as a structural template, since this homologous system also assembles with a 3:6:3 stoichiometry [41]. The resultant MtrCDE model is shown in S7 Fig. We found that two MtrC monomers significantly contact the periplasmic cleft of each MtrD monomer. As shown in S7A Fig, one monomer sits atop the entrance of the periplasmic cleft of MtrD (1546.5 $Å^2$ total contact area), and one contacts the outer surfaces of the PN1 domain (909.3 $Å^2$ total contact area). The positioning of MtrC would prevent substrates from diffusing directly through the top of the entrance to the periplasmic cleft. However, due to its extensive contacts with the entrance of the periplasmic cleft, it is possible that MtrC plays a role in screening of substrates, particularly those of large molecular weight.

To investigate the potential role of MtrC in substrate recognition, our fully assembled MtrC model was subjected to analyses of the Molecular Lipophilicity Potential (MLP) and the Electrostatic Potential (EP) isosurfaces as previously described. We found that the regions of MtrC that contact the periplasmic cleft, and particularly those that might contact bulky substrates, are a mosaic of weakly hydrophilic or neutral surfaces (S7B-C Fig). However, our docking studies exclusively identified docking poses within the lower regions of the periplasmic cleft (S3 Fig) well separated from the MtrC contact regions, raising the question of whether a substrate might contact these regions of MtrC at all. Additionally, docking studies performed by Chitsaz et al. predicted binding poses for AZY almost exclusively within the Deep Pocket (i.e. behind the G-Loop) of the unequilibrated MtrD crystal structure (4MT1) [9]. Even though both docking studies of AZY against MtrD fully sampled the Access Pocket, neither we nor Chitsaz et al. identified predicted binding poses of AZY in the regions of the cleft entrance that contact MtrC. Therefore, based upon the MtrCDE model and the best available evidence, we conclude that MtrC is unlikely to play a significant role in the identification and filtering of substrates.

bioRxiv preprint doi: https://doi.org/10.1101/2021.02.24.432727; this version posted February 24, 2021. The copyright holder for this preprint (which was not certified by peer review) is the author/funder. All rights reserved. No reuse allowed without permission.

AZY diffuses through the periplasmic cleft in a long timescale simulation.

Crystal structures of AcrB suggest that large substrates first associate with the G-Loop after entering the periplasmic cleft, and subsequently enter the Deep Pocket during the Access to Binding transition. MD studies of AcrB also suggest that the energy-requiring step in the conformational sequence is the structural change between the Binding and Extrusion conformations [14-16, 35]. In light of these data, we postulate that our AZY-bound MtrD system approximates a model of MtrD in the Access conformation with a substrate bound at the proximal site, and closely associated with the G-Loop.

The structural transitions of the MtrD efflux cycle are slow and presumably powered by changes in the protonation state of the proton relay network (PRN) [17]. To overcome these limitations, we used TMD to model the conformational changes of a putative transport cycle without altering the protonation state of the transmembrane PRN. However, the applications of TMD can be limited due to the use of biasing forces and the lack of control over simulation timescales, depending upon the TMD implementation used. To address these limitations, we performed an unbiased simulation of AZY_{neu} at Start Site 1 using the AMBER pmemd-cuda MD engine. This 1.5μs simulation was performed at 310K (Fig 7A), and no external forces were applied to any atom in this system; in addition, the protonation states of the PRN were unaltered. Previous work suggests that the transition from Binding to Extrusion is the energy-requiring step in the transport cycle [14]. Therefore, in an unbiased simulation of AZY at Start Site 1, we do not expect the monomer to adopt the Extrusion (or Intermediate) conformation and extrude AZY.

bioRxiv preprint doi: https://doi.org/10.1101/2021.02.24.432727; this version posted February 24, 2021. The copyright holder for this preprint (which was not certified by peer review) is the author/funder. All rights reserved. No reuse allowed without permission.

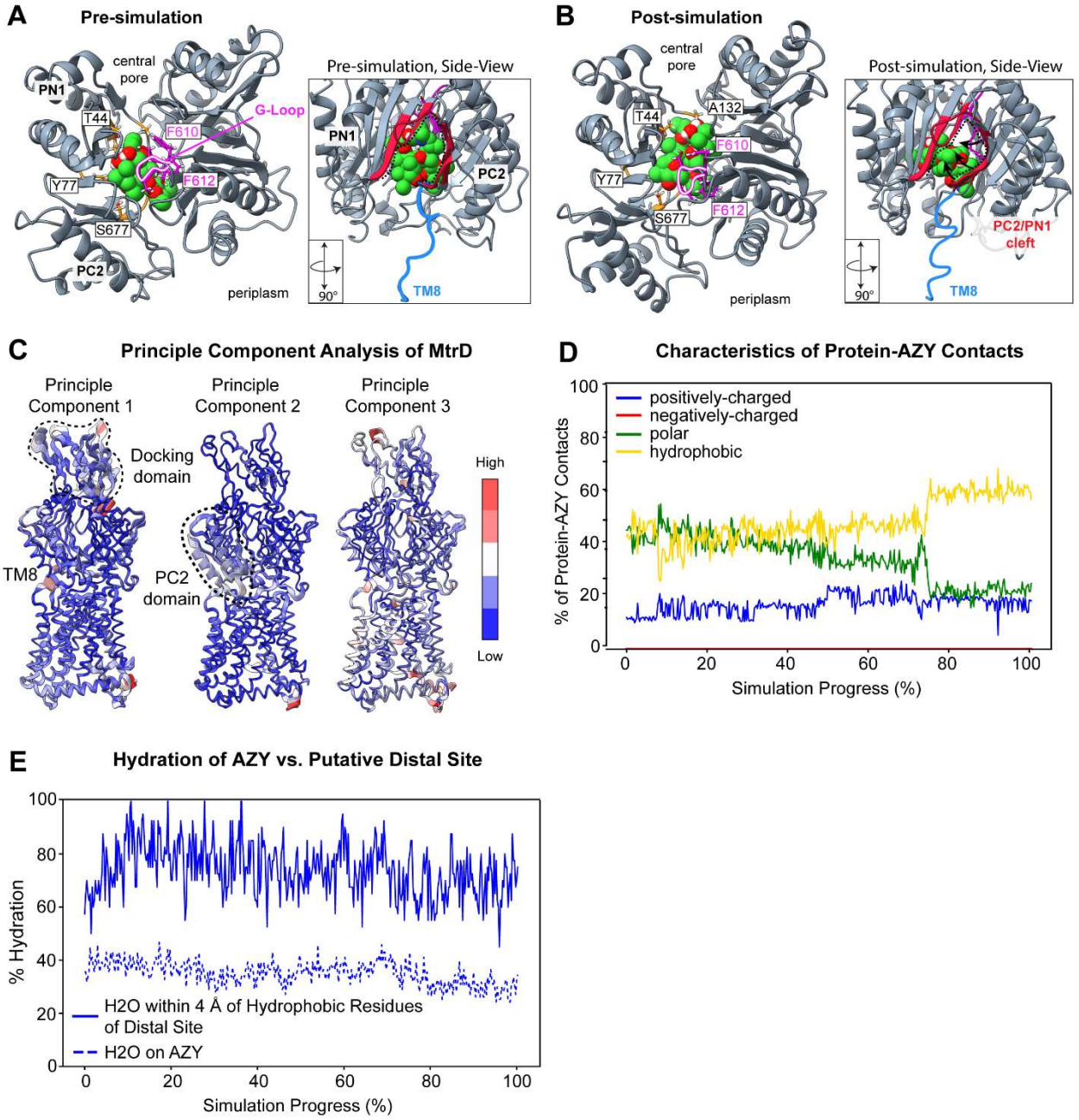

Fig 7. Conformational Dynamics of Azithromycin and MtrD during a Long Timescale MD Simulation. (A-B) Pre- and post-simulation snapshots of AZY_{neu} and the periplasmic cleft, viewed from the top down, or viewed from the side (boxed view), showing AZY (green), the G-Loop (magenta), TM helix 8 (blue), and the PC2/PN1 cleft (outlined in red). Labeled residues interact with AZY for ~80% of the simulation. In (B), arrows show how the PC2/PN1 cleft shifts. (C) Results of Principle Component Analysis on the MtrD backbone. Principle components 1, 2 and 3 mapped onto the MtrD monomer. Red indicates areas of high structural fluctuation; blue indicates very low structural fluctuation. (D) The percentage of contacts between AZY and the periplasmic cleft that are charged, polar, or hydrophobic. (E) The hydration of the SASA of AZY or residues of the putative distal site throughout the simulation.

In this long timescale, unbiased simulation, we observed the movement of AZY past the G-Loop and into the Deep Pocket of MtrD (Fig 7B, Table 3). Principle Component Analysis of the protein backbone

bioRxiv preprint doi: https://doi.org/10.1101/2021.02.24.432727; this version posted February 24, 2021. The copyright holder for this preprint (which was not certified by peer review) is the author/funder. All rights reserved. No reuse allowed without permission.

607 reveals that significant fluctuations occurred in the PC2 domain, TM helix 8, and the docking domain of
608 MtrD (Fig 7C). Since MtrCE is absent from our simulations, fluctuations of the docking domain – which
609 normally interfaces with the sizeable MtrCE complex – are unsurprising (S7 Fig). However, structures of
610 AcrB and the variant $MtrD_{CR103}$ (PDB IDs 5NC5, 6VKT) suggest that conformational changes in TM8 and
611 the PC2 domain do occur, at some point, during the transition from Access to Binding [13, 41]. Specifically,
612 1) the upper portion of TM8 will adopts a more ordered structure, eventually settling into a full alpha helix
613 in the Extrusion conformation; and 2) the PC2 domain opens even wider than in the Access conformation.
614 Interestingly, we observed corresponding conformational shifts in both TM8 and PC2 in our simulation
615 (Fig 7B,C) [13, 41]. Specifically, TM8 transitioned from a disordered loop, to a more ordered structure
616 (Figure 7A,B in blue), and PC2 opened wider once AZY slipped into the DP (S5 Movie).
617

		Percent (%) of Protein-Ligand Contacts Contributed by Domain or Region							
	Simulation Checkpoint	**G-Loop**	**PC1**	**PC2**	**PN1**	**PN2**	**F-Loop**	**AP (PC1 and PC2)**	**DP (PN1 and PN2)**
AZY_{neu}	0%	12.3	12.3	34.4	36.2	1.2	3.7	50.3	37.4
	20%	16.0	4.6	35.1	44.3	0.0	0.0	39.7	44.3
	40%	18.1	4.3	35.1	37.8	4.8	0.0	39.4	42.6
	60%	15.3	6.7	33.7	36.8	7.4	0.0	40.5	44.2
	80%	13.6	17.9	14.2	40.1	11.7	2.5	34.6	51.9
	100%	11.2	16.5	14.1	43.5	11.8	2.9	33.5	55.3

618
619 **Table 3. Percentage of Protein-AZY Contacts Contributed by Specific Domains of the MtrD**
620 **Periplasmic Cleft in a Long Timescale Simulation.** Contacts are defined as residues whose α-carbon is
621 within 4 Å of AZY at each specified timepoint of the 1.5μs simulation with AMBER. Individual domains
622 of the periplasmic cleft are as defined in [13], and the % protein contacts for the Access Pocket (PC1 and
623 PC2) and Deep Pocket (PN1 and PN2) are calculated from the mean contact value. Contact analysis was
624 performed with scripts in *Tcl* and python.
625

626 Furthermore, while many of the MtrD-AZY contacts were either hydrophobic or polar at the
627 beginning of the simulation, the majority of contacts were hydrophobic at the end of the simulation (Fig
628 7D). The hydration of the $SASA_{AZY}$ decreases slightly overall; however, the $SASA_{distal}$ is ≥ 70% hydrated
629 for the majority of the simulation, indicating that significant hydrophobic interactions between the putative
630 distal site and AZY were then unlikely to occur in our simulation (Fig 7E). The movement of AZY through
631 the periplasmic cleft, along with the accompanying conformational shifts of MtrD, are shown in Movie S5.
632 Our results are in line with MD studies of the MtrD homologue AcrB, which suggest that the transition

bioRxiv preprint doi: https://doi.org/10.1101/2021.02.24.432727; this version posted February 24, 2021. The copyright holder for this preprint (which was not certified by peer review) is the author/funder. All rights reserved. No reuse allowed without permission.

from Binding to Extrusion is the energy dependent phase [35]. Our results are also supported by the MD study of MtrD performed by Chitsaz et al, in which progesterone was observed to spontaneously move into Access Pocket, past the G-Loop, and into the Deep Pocket – all in the absence of biasing forces, and without changes to the Proton Relay Network of MtrD [9]. Interestingly, this study observed the movement of progesterone through the periplasmic cleft in ~40 ns; we postulate that the increased movement speed (relative to our simulation of AZY) could be due to the significant discrepancy in size between progesterone and AZY (~315 Da for progesterone vs. ~749 Da for AZY).

Discussion

In this study, we have simulated the transport of AZY by MtrD in biased Targeted Molecular Dynamics simulations, and in an unbiased, long-timescale NPT MD simulation. We also observed the passive rejection of SRY from the entrance of the periplasmic cleft, or alternatively the retention of SRY within the cleft during the putative transport cycle. We showed that the access to various isosurfaces of the periplasmic cleft changes dynamically, and that access is controlled in a way that might facilitate substrate discrimination, transport and extrusion. In contrast to the interpretation of results from crystal structures of the MtrD homologue AcrB and cryo-EM structures of $MtrD_{CR103}$, AZY was not observed to interact with residues of the putative distal binding site in the Deep Pocket in TMD simulations, but took an alternative transport pathway mediated by water, and by interactions with PN1 and the G-Loop [13, 16]. In our long timescale, unbiased MD simulation, we observed AZY diffuse into the Deep Pocket past the G-Loop, and we observed the AZY-bound monomer begin to undergo conformational changes that are associated with the transition from Access to Binding.

AZY TMD trajectories diverge during the transition from access to binding

With our TMD simulations, we were able to increase the sample size significantly to 20 simulations per ligand at each starting site. This larger sample size allowed us to observe variable behavior of AZY during the simulations. Through analysis of the specific domains contacted by AZY throughout the simulation, we found that the “Transport” trajectories diverged from the “Non-Transport” trajectories

bioRxiv preprint doi: https://doi.org/10.1101/2021.02.24.432727; this version posted February 24, 2021. The copyright holder for this preprint (which was not certified by peer review) is the author/funder. All rights reserved. No reuse allowed without permission.

during the transition from Access to Binding (Table 1). Specifically, if AZY slipped past the G-Loop at some point during the transition from Access to Binding, then AZY was positioned fully behind the G-Loop, and subsequently squeezed towards the exit as the cleft entrance closes (during the transition from Binding to Extrusion). Notably, this movement of AZY into the Deep Pocket occurred during the conformational transition period, and thus *before* the periplasmic cleft had fully adopted the Binding conformation. These data indicate that AZY can pass the G-Loop even if the cleft is not in its most open conformation. This correlates with the results of our long timescale simulation, in which AZY spontaneously slipped past the G-Loop and into the Deep Pocket, even though the transporter was not yet in the Binding conformation. This is also supported by the results of our docking experiments against apo-MtrD, which identified predicted binding positions of AZY that spanned the length of the periplasmic cleft (S3 Fig).

Molecular characteristics of the periplasmic cleft facilitate recognition and diffusion of substrates

Our MLP analyses revealed that the available MLP isosurfaces of the periplasmic cleft changes dynamically throughout the transport cycle. Areas that are responsible for substrate filtration and capture contain significantly hydrophobic isosurfaces, and in the case of the alternate entryway site for small substrates, the passage is lined with bulky hydrophobic residues (Fig 5). These lipophilic isosurfaces may facilitate the substrate selectivity of MtrD, which is a member of the hydrophobic-amphiphile family of RND transporters, thereby allowing ligands with sufficient complementarity to enter the cleft and associate with the G-Loop. As shown with our simulations of SRY, bulky molecules with non-complementary characteristics are unable to pass reliably through this selectivity filter at the cleft entrance.

The MLP isosurfaces of the periplasmic cleft interior are mosaic-like; consequently, they are well-suited to allowing MtrD substrates to diffuse through the tunnel formed by the periplasmic cleft, as shown by Chitsaz et al. in their simulations of MtrD and its substrate progesterone [9]. Along with the presence of water [35], these mosaic-like surfaces of the interior may prevent substrates from stabilizing inside the cleft as subsequent conformational motions squeeze them towards the funnel domain. Once substrates reach the

bioRxiv preprint doi: https://doi.org/10.1101/2021.02.24.432727; this version posted February 24, 2021. The copyright holder for this preprint (which was not certified by peer review) is the author/funder. All rights reserved. No reuse allowed without permission.

Deep Pocket behind the G-Loop, access to lipophilic areas in the Access Pocket is restricted by closure of the PC1/PC2 domains. With the exception of the lipophilic stop-gap formed by the G-Loop, the ligand-accessible isosurfaces are either hydrophilic-neutral or positive neutral (Figures 5 and 6, Panel A, 'Extrusion'). The positive patch may repel charged substrates from the center of the cleft, thereby positioning substrates for release into the funnel domain.

Thus, the interior of the cleft contains 1) substrate-complementary surfaces to aid discrimination at the entrance, 2) mosaic-neutral surfaces to aid diffusion towards the funnel domain, and 3) mosaic-repulsive surfaces to aid diffusion and eventual extrusion of substrates. The correlated motions of the periplasmic cleft and of the G-Loop serve to alternately restrict and allow access to areas with specific MLP and EP signatures. While the MLP signatures of the cleft do not appear to change significantly in the presence of AZY, the presence of AZY does appear to affect the EP isosurfaces of the cleft.

AZY did not exit fully into the funnel domain

We did not observe the exit of AZY into the funnel domain (Fig 1A-B) in any of our MD simulations. To our knowledge, no computational simulation of an RND transporter has modeled substrate release into the funnel/docking domain without the use of biasing forces upon the ligand or substrate itself [9, 45], which is consistent with the hypothesis that substrate release occurs on a longer timescale than is currently reasonable to simulate on most systems.

AZY did not interact with the 'hydrophobic trap' of the distal site in our simulations

Cryo-EM structures of $MtrD_{CR103}$ show the macrolide erythromycin bound in the "hydrophobic trap" of the PC1/PN2 cleft (PDB 6VKT) [13, 16]. The 'hydrophobic trap' is a set of hydrophobic residues that forms the alternate entry site for small, hydrophobic substrates in the Deep Pocket (Fig 2C, green residues) [46]. Studies suggest that residues of the hydrophobic trap are quite important for the proper function of RND transporters [46, 47]; specifically regarding MtrD, mutations in this region (F136A,

bioRxiv preprint doi: https://doi.org/10.1101/2021.02.24.432727; this version posted February 24, 2021. The copyright holder for this preprint (which was not certified by peer review) is the author/funder. All rights reserved. No reuse allowed without permission.

F176A, and F623C) correlate with a decrease in the MIC (Minimum Inhibitory Concentration) of the antibiotics rifampin (~823 Da), novobiocin (~613 Da), and oxacillin (~401 Da) [9]. Since none of these antibiotics are macrolides, the result of mutations in this region upon the MIC of macrolides warrants further study. Consequently, we expected that AZY would interact with the hydrophobic residues of the distal site when the transporter was in the Binding conformation.

Surprisingly, in our TMD simulations, we found that AZY took an alternate path through the Deep Pocket primarily involving PN1 and the G-Loop, and not PN2 and the hydrophobic trap as expected. In our long timescale simulation, we observed interactions between AZY and the hydrophobic trap only at the end of the simulation, and these contacts were relegated to the periphery of the AZY molecule. At no point, in any of our simulations, was AZY bound in a conformation similar to that of erythromycin in the Deep Pocket of $MtrD_{CR103}$. Nevertheless, the role of the distal site (and the hydrophobic trap therein) in macrolide transport is of interest. One particularly important question that remains is whether the conformational change from Binding to Extrusion is enough to extrude a large substrate out of the hydrophobic trap and into the funnel domain?

To investigate this question, we modeled the structural transition from Binding to Extrusion using the erythromycin-bound monomer of $MtrD_{CR103}$ (PDB ID 6VKT, Movie S6). We found that the putative distal site constricts significantly during this conformational change. We note that this constriction may be sufficient to squeeze a bulky substrate up into position for release into the funnel domain, but it is unclear whether it provides enough force to extrude the substrate. Therefore, it remains unclear whether the substrate exits into the funnel domain as the monomer transitions from Binding to Extrusion, or if the monomer adopts Extrusion and then waits for the substrate to disassociate. Our data suggest that substrate release into the funnel domain occurs slowly and *after* the monomer has reached Extrusion. Furthermore, our data indicate that the extrusion of bulky substrates may be aided by further constriction of the periplasmic cleft in the putative Intermediate (aka “Resting”) state.

bioRxiv preprint doi: https://doi.org/10.1101/2021.02.24.432727; this version posted February 24, 2021. The copyright holder for this preprint (which was not certified by peer review) is the author/funder. All rights reserved. No reuse allowed without permission.

Molecular characteristics of the periplasmic cleft facilitate rejection of SRY

Our results demonstrate that SRY is unlikely to successfully enter the periplasmic cleft of MtrD, and thus will not be transported by MtrD. Since SRY is too large to pass through the alternate entry site behind the G-Loop, the only available point of entry is through the Access Pocket (AP) at the foremost region of the periplasmic cleft. Our simulations of SRY at the periplasmic cleft entrance (Fig 2B, Site 2) support the conclusion that SRY is unlikely to successfully enter through the Access Pocket of MtrD. Nevertheless, while SRY was observed to diffuse out of the cleft and into the solvent, it did remain associated with the periplasmic-exposed surfaces of the AP (S6B Fig, S4 Movie). The outer surfaces of the AP possess negative patches, particularly near D709, that may attract SRY to these regions once it exits the cleft. Taken together, our results also indicate that SRY is an unlikely candidate for an MtrD inhibitor, since it is unable to enter the transporter successfully.

Mutations alter the molecular landscape of the periplasmic cleft

Mutational studies have shown that a K823E mutation in the periplasmic cleft results in a fourfold increase in AZY resistance; consequently, K823 is thought the be important for macrolide recognition [9, 13]. We performed EP and MLP analysis of the MtrD periplasmic cleft with the K823E mutation and found that the cleft gains a strongly negative patch in the proximal binding site near the G-Loop and TM8. Since >90% of AZY are weakly positively charged at physiological pH, it is possible that this pocket would serve to further attract AZY into the periplasmic cleft after the initial association with the entrance of the cleft. Indeed, we observed close interactions between AZY and K823 throughout the majority of the long timescale simulation. Consequently, K823-macrolide interactions warrant further study.

Analysis of the K823E mutation raises an additional question: could $MtrD_{K823E}$ transport SRY? When examining the MLP of the periplasmic cleft entrance, we found that PC1, which forms half of the entrance to the cleft, contains significant hydrophobic isosurfaces (Fig 5A-B). Positioned opposite to the hydrophobic surfaces of PC1 is the conserved, positively charged residue R714. Thus for SRY to successfully enter the periplasmic cleft, it would need to pass the positively-charged residue R714, as well as the significantly hydrophobic isosurfaces of PC1, before reaching the K823E. As shown in S1 Table, the

bioRxiv preprint doi: https://doi.org/10.1101/2021.02.24.432727; this version posted February 24, 2021. The copyright holder for this preprint (which was not certified by peer review) is the author/funder. All rights reserved. No reuse allowed without permission.

765 topological polar surface area (TPSA) of SRY is nearly two times greater than the TPSA of AZY_{h2}. In this
766 case, as TPSA increases, hydrophilicity increases, and vice versa. Analysis of the Log *S* (solubility in water)
767 and the Log $P_{oct/wat}$ (octanol-water partitioning) reveals that SRY is significantly more hydrophilic than any
768 of the three protonation states of AZY (S1 Table). Therefore, SRY is unlikely to interact favorably with the
769 hydrophobic surfaces of PC1, or with R714 of PC2. Since AZY is significantly more lipophilic than SRY,
770 AZY is more likely to interact favorably with these surfaces, and to successfully enter the periplasmic cleft.
771 To our knowledge, the potential of $MtrD_{K823E}$ to transport SRY has not been assessed.
772

773 The potential effects of different forcefields on simulations of AZY and MtrD

774 In this study, we demonstrated the transport of AZY, a known substrate of MtrD, in simulations
775 with two types of force fields using two different MD engines – NAMD with CHARMM36 force fields,
776 and AMBER pmemd-cuda with Amber force fields. This suggests that our results are not artifacts of the
777 force fields employed.
778

779 MtrD transports substrates through a combination of controlled diffusion and 780 peristalsis

781 On the basis of this work, we suggest the following transport mechanism for macrolides by MtrD.
782 (1) A transported macrolide first associates with, and then passes, the selectivity filter at the entrance of the
783 periplasmic cleft. This filter is formed by conserved residues and by isosurfaces that are complementary to
784 the substrate profile of the transporter. (2) The macrolide diffuses slowly through the periplasmic cleft,
785 contacting residues of the loosely defined proximal site, and eventually associating with the G-Loop (Fig
786 2A) [13]. (3) The macrolide slips past the G-Loop and into the Deep Pocket, still associating with residues
787 of the proximal site. Once the macrolide enters the Deep Pocket, the MtrD monomer undergoes the
788 transition from Access to Binding, opening the periplasmic cleft even wider. (4) Once in the Deep Pocket,
789 the macrolide may interact with the putative distal site, or with the PN1 domain. In both cases, it is still
790 contacting the G-Loop. If the macrolide takes the 'PN1 route', it is technically still associating with residues

bioRxiv preprint doi: https://doi.org/10.1101/2021.02.24.432727; this version posted February 24, 2021. The copyright holder for this preprint (which was not certified by peer review) is the author/funder. All rights reserved. No reuse allowed without permission.

of the proximal binding site (Fig 2A). (5) Changes in the transmembrane Proton Relay Network then power the transition from Binding to Extrusion, in part through resultant vertical shearing motions in the transmembrane helices [15]. This restricts access to the periplasm and the Access Pocket, resulting in the extrusion of the substrate towards the funnel domain. (6) Once the monomer reaches the Extrusion conformation and the substrate is positioned for disassociation into the funnel domain, the monomer waits for the relatively slow process of substrate release. (7) During this waiting period, the monomer could relax and pass through the putative Intermediate conformation, which may serve to further move bulky substrates out of the transport channel. It is unclear whether MtrD requires multiple cycles to transport a ligand as large as AZY. It is also unclear if the presence of multiple transport ligands within the same periplasmic cleft, or in other monomers of the transporter, would aid the dissociation of AZY into the funnel domain.

Multiple transport pathways through the periplasmic cleft

In conclusion, our data suggest that substrate transport through the periplasmic cleft of MtrD depends upon a combination of diffusion, gated access to areas with variable charge and lipophilicity isosurfaces, and conformational changes of the surrounding structure. We may have identified a low energy, peristalsis-complementary diffusion path for AZY through the periplasmic cleft that does not involve interactions with the hydrophobic trap of the putative distal site [16]. Our results suggest that multiple pathways, or residue contact pathways, may exist within the periplasmic cleft for substrates of MtrD.

bioRxiv preprint doi: https://doi.org/10.1101/2021.02.24.432727; this version posted February 24, 2021. The copyright holder for this preprint (which was not certified by peer review) is the author/funder. All rights reserved. No reuse allowed without permission.

Acknowledgements

The authors would like to acknowledge and thank James W. McCormick for his valuable and constructive suggestions and guidance during the planning and development of this work. We would also like to thank Amit Kumar and Robert Kalescky for their continual support, guidance, and patience with our use of the *Maneframe II* computer. We would like to thank Dr. Edward Yu for piquing our interest in these fascinating transporters.

The authors declare no competing financial interest.

bioRxiv preprint doi: https://doi.org/10.1101/2021.02.24.432727; this version posted February 24, 2021. The copyright holder for this preprint (which was not certified by peer review) is the author/funder. All rights reserved. No reuse allowed without permission.

Materials and Methods

Software

Missing residues in the 4MT1 structure of MtrD were repaired with Modeller v. 9.24 (residues 1, 494-507, 671-672, 1041-1056) [6, 29]. The complete MtrD homotrimer was built in VMD (Visual Molecular Dynamics, v 1.9.4) using the crystallographic coordinates in the 4MT1 PDB file [48]. A heterogeneous bilayer consisting of POPE, POPG, and cardiolipin was created using the CHARMMGUI Membrane Builder with CHARMM36 topology [24, 49, 50]. The homotrimer was minimized to relax the modeled loops, and then embedded into the membrane using coordinates from the Orientation of Proteins in Membranes (OPM) Michigan database [38]. Lipids were retained in the central pore of the protein. The protein-membrane system was solvated with TIP3 water and ionized to a concentration of 0.15M NaCl using the Solvate and Autoionize plugins of VMD. All Molecular Dynamics (MD) simulations were performed with NAMD 2.12 using CHARMM36 force fields and topology unless otherwise stated. The 1.5 µs simulation of MtrD and AZY was performed with AMBER18 using the ff14SB, Lipid17, GAFF2 and TIP3p force fields employing the pmemd.cuda-DPFP molecular dynamics engine [22, 23, 27]. The CHARMM-GUI Ligand Reader and Modeller was used to format and parameterize ligands for simulations [24, 49]. PROPKA3.1 and the Henderson-Hasselbalch Equation was used to estimate ligand protonation states at a pH of 7.4. *Autodock Vina 1.1.2* was used to dock AZY or SRY ligands to the drug binding domain of MtrD. Autodock Tools was used to define dock boxes [28, 51]. Bio3D was used for analysis and generation of target structures for Targeted MD simulations [52]. Protein images were generated using UCSF ChimeraX [53]. Data analysis was performed using in-house scripts written in *Tcl,* R, and python. Figures were prepared with Adobe Illustrator. Movies were prepared with ChimeraX, VMD, and Adobe Procreate.

Ligand docking to the drug binding pocket of MtrD

bioRxiv preprint doi: https://doi.org/10.1101/2021.02.24.432727; this version posted February 24, 2021. The copyright holder for this preprint (which was not certified by peer review) is the author/funder. All rights reserved. No reuse allowed without permission.

To generate a starting position for our ligands of interest, we docked azithromycin and streptomycin with the periplasmic cleft of wild-type MtrD. The structures of the MtrD substrate azithromycin (AZY) and the non-substrate streptomycin (SRY) were downloaded from PubChem and converted to 3D structures using OpenBabel v. 2.3.2 [54]. The full-length (repaired) MtrD monomer and ligands were converted to PDBQT files using AutoDock Tools v. 1.5.6 [51]. AutoDock Vina 1.1.2 was then used to dock each ligand with four overlapping boxes that encompassed the entire periplasmic cleft of MtrD (S2 Fig) [28]. The docking exhaustiveness parameter was set to 128 replicates to ensure reasonable coverage of the docking regions; default exhaustiveness for Autodock Vina is 8. Docking results were processed using in-house bash scripts, producing the top 9 poses of each ligand per dock box, ranked by binding affinity (S3 Fig).

To select ligand start sites for MD simulations, the resultant docking poses were then processed using AutoDock Tools. *The purpose of the docking experiments was to generate a plausible starting position for the ligand within the periplasmic cleft, not to evaluate individual estimated binding affinities.* Vina has an estimated standard error in calculating binding energies for small molecule redocking experiments of 2.85 kcal/mol [28]. Similar experiments for calculating the standard errors of affinity estimates for peptide- or protein-ligand complexes is expected to be much higher, due in large part to the significantly greater conformational degrees of freedom allowed for the ligand of interest. Consequently, the top 9 docking poses were evaluated according to position within the periplasmic cleft, and not to individual estimated affinities. We found that the overlapping dock boxes produced some identical docking poses (S3 Fig); from each cluster of identical poses, one representative pose was selected randomly. After the elimination of identical poses, three poses were selected for both AZY and SRY. For MD simulations with each ligand, we selected one docking pose at the Mid-Point of the cleft but within the proximal binding site – this became Start Site 1. We chose a second pose at the entrance of the periplasmic cleft – this became Start Site 2. The PDBQT files of ligands in each selected pose were converted to PDB format and "all atom" representations using Open Babel 2.3.2, since the PDB to PDBQT processing (for docking) removes all non-polar hydrogens [54].

The CHARMMGUI Ligand reader and Modeler were then used format the ligands as PDBs, to create parameter files for simulations with NAMD or AMBER, to create various protonation states if

bioRxiv preprint doi: https://doi.org/10.1101/2021.02.24.432727; this version posted February 24, 2021. The copyright holder for this preprint (which was not certified by peer review) is the author/funder. All rights reserved. No reuse allowed without permission.

applicable (S4 Fig), and to check for stereochemistry issues [24, 49]. Using available data (if possible) and analyses with Propka3.1 and OpenBabel, ligand protonation states were assessed at a physiologically relevant pH of 7.4 [54, 55]. At this pH, according to our calculations, SRY is a triple cation with only ~0.02% of molecules being double cations at pH 7.4. Therefore, we simulated the completely protonated form of streptomycin (SRY). For azithromycin (AZY), there are two ionizable sites (S4 Fig). For the first ionizable site, the pKa is ~8.5-8.74, meaning that ~4.6-7.9% of AZY are unprotonated at a pH of 7.4 [31, 56]. For the second site, the pKa is 9.45, meaning that ~1% of AZY are unprotonated at this site [31]. Since it is thought that the neutral, unprotonated form of AZY may more readily diffuse through cell membranes, we included all three protonation states of AZY in our simulations.

We note also that pKa values may change depending upon the surrounding environment, and that the pKa of amines – of which there are two present on AZY – is expected to increase when moving from an aqueous to a more hydrophobic environment. This may result in higher percentages of the unprotonated form of these AZY in more hydrophobic environments. While these environments may increase the proportion of the unprotonated species of AZY, they are not expected to significantly change the protonation state of SRY (S4 Fig).

TMD simulations of the ligand free system with NAMD

TMD simulations, and the unbiased relaxation MD simulations that preceded TMD, were performed using NAMD 2.12 with the CHARMM36 forcefield, a timestep of 2 fs, and a non-bonding cutoff of 12 angstroms [25, 50]. Simulations were performed with constant temperature and pressure (NPT) in a periodic cell using Langevin temperature and pressure control, and Particle Mesh Ewald electrostatics. The temperature was maintained at 310K. As preparation for subsequent docking experiments and TMD simulations, the ligand-free system was minimized, heated to 310K, and equilibrated for 100 ns. An equilibrated MtrD monomer was extracted from the end of the final simulation and used for docking ligands, and also for aligning target structures for TMD simulations.

bioRxiv preprint doi: https://doi.org/10.1101/2021.02.24.432727; this version posted February 24, 2021. The copyright holder for this preprint (which was not certified by peer review) is the author/funder. All rights reserved. No reuse allowed without permission.

Preparing the protein-ligand system

After docking, each ligand was converted to a PDB and then uploaded, checked for structural or conformational issues, and parameterized using the CHARMM-GUI Ligand Reader and Modeller. After adding the ligand into the system and removing any overlapping water molecules using VMD, the new system was minimized, heated to 310K, and equilibrated in unbiased MD simulations for 50 ns. Using a short TMD simulation, the alpha carbons of the equilibrated system were then guided to the starting coordinates of the 4MT1 crystal trimer.

Targeted Molecular Dynamics Simulations with NAMD

To mimic a putative drug transport cycle of MtrD, TMD simulations were performed as previously described [57, 58] using target coordinates derived from structures of MtrD homologue(s) (S1 Fig). In our TMD simulations, alpha carbons of the protein backbone are guided to ≤ 0.7 Å of the target coordinates. Forces are not applied to the ligand of interest, and protein sidechains move freely. When simulations were performed, no published structures of MtrD in various conformations were available, so we used structures derived from AcrB from *E. coli,* which shares a sequence identity of 48.6%, and CmeB from *C. jejuni*, which shares a sequence identity of 38.07%, with MtrD. Structures used for TMD simulations were the 4DX5 (1.9 Å) and 5NC5 (3.2 Å) structures of AcrB, and the 5LQ3 (3.5 Å) structure of CmeB (S1 Fig). A comparison of e normal ("wildtype") MtrD, $MtrD_{CR103}$, and the structures used in our TMD simulations, is provided in S9 Fig. Using the structurally homologous Cα atoms of MtrD for each structure, target structures were superposed with the equilibrated MtrD-ligand system using the Bio3D module of R.

In subsequent TMD simulations on equilibrated protein-ligand systems, forces were applied using in-house *tcl* scripts in NAMD [58]. These forces were applied to selected Cα atoms of the ligand-bound protomer to gently guide the Cα atoms toward the respective target coordinates. The magnitudes of these forces were inversely proportional to the RMSD (root mean squared deviation) of the distances separating the selected Cα atoms from their target coordinates. Cα atoms were pushed to ≤ 0.7 Å of their target coordinates. Significant steric clashes were not observed between protomers, even though only one protomer was guided through conformational changes. Analysis of the protein-ligand interactions for each

bioRxiv preprint doi: https://doi.org/10.1101/2021.02.24.432727; this version posted February 24, 2021. The copyright holder for this preprint (which was not certified by peer review) is the author/funder. All rights reserved. No reuse allowed without permission.

system were performed using *tcl* scripts in VMD and the Bio3D R module. At equal intervals throughout each simulation, the number and characteristics of ligand-protein contacts were determined. Results are reported either for individual simulations or the averages for all twenty simulations.

We simulated three protonation states of the MtrD substrate azithromycin (AZY): AZY_{neu}, a neutral, unprotonated form of azithromycin; AZY_{h1}, a singly protonated, positively charged form of azithromycin; and AZY_{h2}, doubly protonated, positively charged form of azithromycin (S4 Fig). As a negative control, we tested streptomycin (SRY), a known non-substrate of MtrD, and a triple cation at physiological pH. Two start sites were tested for each ligand –Site 1, in which the ligand was located in between the AP and the DP near the G-Loop, and was associating with the proximal binding site, and Site 2, in which the ligand was at the entrance of the periplasmic cleft, and was associating with the foremost residues of the proximal binding site (Fig 2).

The center of mass coordinates, and ligand RMSDs from starting positions, were calculated using Tcl scripts in VMD. Protein-ligand systems were oriented such that the membrane is in the X – Y coordinate plane; therefore, *positive* vectorial movement along the X axis indicates movement through the periplasmic cleft *towards* the central region of MtrD, as would be expected during ligand transport. In contrast, *negative* vectorial movement along the X axis indicates movement *away* from the central region and towards the periplasm. Since biased external forces were not applied to the ligand, any movement through the protein should only be dependent upon the conformational changes of the MtrD protein and the limited diffusional possibilities of the transport substrate, which are dependent on the protein conformations.

A long timescale MD simulation of AZY-bound MtrD

Using the AMBER pmemd-cuda MD engine, we performed a GPU-accelerated, 1.5 µs simulation of the MtrD homotrimer with AZY_{neu} bound at Site 1 in the periplasmic cleft [23]. The ligand was parameterized with AMBER antechamber using the GAFF2 force field, and the protein-ligand system was built in AMBER tLEAP [23, 59, 60]. Except for parameterization files, the system was identical in composition and size to the system run with NAMD, except that the membrane did not contain cardiolipin; the heterogeneous membrane (POPE/POPG only), water, and ions were maintained. The system was first

bioRxiv preprint doi: https://doi.org/10.1101/2021.02.24.432727; this version posted February 24, 2021. The copyright holder for this preprint (which was not certified by peer review) is the author/funder. All rights reserved. No reuse allowed without permission.

relaxed in unbiased equilibration MD simulations for 200ns, and then allowed to run freely for a total of 1.5 µs. Analysis was performed using AMBER cpptraj, UCSF ChimeraX, the PDB2PQR server, in-house Tcl scripts with VMD or with python, and with Bio3D in R [23, 26, 48, 52, 53, 61].

Molecular Lipophilicity Potential

The molecular lipophilicity potential (MLP) describes the three-dimensional distribution of lipophilicity across the molecular surface of a molecule or protein. The MLP at a point in space (k) can be calculated using the following equation [42], where N is the number of molecular fragments, F_i is the lipophilic contribution of each molecular fragment (i), and the distance function $f(d_{ik})$ describing the distance between the point (k) to the molecular fragment *i*:

$$MLP_k = \sum_{i=1}^{N} F_i \cdot f(d_{ik})$$

The sum of all MLP values for the molecular surfaces of the periplasmic cleft yields the Lipophilic Index (LI) of that region, defined as:

$$LI = \frac{\sum MLP^+}{\sum MLP^+ + |\sum MLP^-|} \times 100$$

MLP^+ denotes regions with a positive, or lipophilic, MLP value; MLP^- denotes regions with a negative, or hydrophilic, MLP value. If the fragmental contributions of the MLP^+ and the MLP^- of a region sum to roughly zero, then the region is classified as MLP "neutral".

Electrostatic Potential

The electrostatic potential (EP) surfaces of the periplasmic cleft were calculated using the APBS/PDB2PQR server and visualized using ChimeraX [61-63]. All EP calculations were performed at 310K with all other Poisson-Boltzmann parameters at default. EP calculations were performed on MtrD

bioRxiv preprint doi: https://doi.org/10.1101/2021.02.24.432727; this version posted February 24, 2021. The copyright holder for this preprint (which was not certified by peer review) is the author/funder. All rights reserved. No reuse allowed without permission.

both in presence and absence of AZY by isolating PDB "snapshots" of the AZY-bound or ligand-free MtrD monomer from specific timepoints in the simulation; subsequent EP calculations were performed on these PDB snapshots using the APBS/PDB2PQR server.

Percent hydration of solvent accessible surface area (SASA)

The percent (%) hydration of the available SASA of each ligand was calculated as follows:

$$\%\ Hydration\ of\ SASA = \frac{\#\ H_2O\ at\ frame\ N}{\#\ H_2O\ of\ Complete\ Hydration\ Layer}$$

With N being the individual frame, or timepoint, analyzed. The complete potential hydration layer describes the number of water molecules that would surround the equilibrated ligand if it was immersed freely in solvent. The complete potential hydration layer was calculated by 1) immersing each ligand into a water box, 2) neutralizing the system with 0.15 mol/L NaCl, 3) minimizing the solvated system and heating it to 310K, and 4) simulating the ligand with free MD for 20 ns. The position of water molecules within three different radii of AZY or SRY (radii of 3 Å, 4 Å, 5 Å, and 6 Å) were assessed to determine which radius describes a complete hydration layer around the ligand of interest. For both AZY and SRY, the optimal radius was water within 4 Å of any atom of the ligand. The number of water molecules to completely hydrate each ligand in its free-MD relaxed state was determined to be as follows: AZY_{neu} , 107 water molecules; AZY_{h1} , 103 water molecules; AZY_{h2} , 104 water molecules; SRY, 83 water molecules. The SASA was calculated using the "measure" function of VMD.

Molecular modeling of the fully-assembled MtrCDE complex

Since the structure of MtrC remains unsolved, we used the structure of the homologous membrane fusion protein AcrA from the AcrAB-TolC RND Efflux system; AcrA shares a 44.6% sequence identity with MtrC (PDB ID 5NG5) [41]. Like AcrAB-TolC, the MtrCDE RND efflux system also assembles with a 3:6:3 stoichiometry, indicating that MtrC assembles as a hexamer [43]. A full model of MtrCDE was

bioRxiv preprint doi: https://doi.org/10.1101/2021.02.24.432727; this version posted February 24, 2021. The copyright holder for this preprint (which was not certified by peer review) is the author/funder. All rights reserved. No reuse allowed without permission.

subsequently built using the structures of apo MtrD (4MT1), open MtrE (4MTO), and the model of MtrC [6, 44]. To assemble MtrCDE with the appropriate stoichiometry and positioning of subunits, we used the structure of fully-assembled AcrAB-TolC (5NG5) was used as a template [41]. The MtrCDE model is shown in S7 Fig. We note that a significant flexible linker, residues 378 - 397, is missing from the 5NG5 structure of AcrA, and therefore the homology model of MtrC.

bioRxiv preprint doi: https://doi.org/10.1101/2021.02.24.432727; this version posted February 24, 2021. The copyright holder for this preprint (which was not certified by peer review) is the author/funder. All rights reserved. No reuse allowed without permission.

References

1. Wade JJ, Graver MA. Survival of six auxotypes of Neisseria gonorrhoeae in transport media. J Clin Microbiol. 2003;41(4):1720-1. Epub 2003/04/12. doi: 10.1128/jcm.41.4.1720-1721.2003. PubMed PMID: 12682168; PubMed Central PMCID: PMCPMC153907.
2. Rowley J, Vander Hoorn S, Korenromp E, Low N, Unemo M, Abu-Raddad LJ, et al. Chlamydia, gonorrhoea, trichomoniasis and syphilis: global prevalence and incidence estimates, 2016. Bull World Health Organ. 2019;97(8):548-62P. Epub 2019/08/07. doi: 10.2471/BLT.18.228486. PubMed PMID: 31384073; PubMed Central PMCID: PMCPMC6653813.
3. Smolarchuk C, Wensley A, Padfield S, Fifer H, Lee A, Hughes G. Persistence of an outbreak of gonorrhoea with high-level resistance to azithromycin in England, November 2014May 2018. Euro Surveill. 2018;23(23). Epub 2018/06/14. doi: 10.2807/1560-7917.ES.2018.23.23.1800287. PubMed PMID: 29897041; PubMed Central PMCID: PMCPMC6152168.
4. Nikaido H. RND transporters in the living world. Res Microbiol. 2018;169(7-8):363-71. Epub 2018/03/27. doi: 10.1016/j.resmic.2018.03.001. PubMed PMID: 29577985; PubMed Central PMCID: PMCPMC6151166.
5. Anes J, McCusker MP, Fanning S, Martins M. The ins and outs of RND efflux pumps in Escherichia coli. Front Microbiol. 2015;6:587. Epub 2015/06/27. doi: 10.3389/fmicb.2015.00587. PubMed PMID: 26113845; PubMed Central PMCID: PMCPMC4462101.
6. Bolla JR, Su CC, Do SV, Radhakrishnan A, Kumar N, Long F, et al. Crystal structure of the Neisseria gonorrhoeae MtrD inner membrane multidrug efflux pump. PLoS One. 2014;9(6):e97903. Epub 2014/06/06. doi: 10.1371/journal.pone.0097903. PubMed PMID: 24901477; PubMed Central PMCID: PMCPMC4046932.
7. Hagman KE, Lucas CE, Balthazar JT, Snyder L, Nilles M, Judd RC, et al. The MtrD protein of Neisseria gonorrhoeae is a member of the resistance/nodulation/division protein family constituting part of an efflux system. Microbiology. 1997;143 (Pt 7):2117-25. Epub 1997/07/01. doi: 10.1099/00221287-143-7-2117. PubMed PMID: 9245801.
8. Unemo M, Shafer WM. Antimicrobial resistance in Neisseria gonorrhoeae in the 21st century: past, evolution, and future. Clin Microbiol Rev. 2014;27(3):587-613. Epub 2014/07/02. doi: 10.1128/CMR.00010-14. PubMed PMID: 24982323; PubMed Central PMCID: PMCPMC4135894.
9. Chitsaz M, Booth L, Blyth MT, O'Mara ML, Brown MH. Multidrug Resistance in Neisseria gonorrhoeae: Identification of Functionally Important Residues in the MtrD Efflux Protein. mBio. 2019;10(6). Epub 2019/11/21. doi: 10.1128/mBio.02277-19. PubMed PMID: 31744915; PubMed Central PMCID: PMCPMC6867893.
10. Warner DM, Shafer WM, Jerse AE. Clinically relevant mutations that cause derepression of the Neisseria gonorrhoeae MtrC-MtrD-MtrE Efflux pump system confer different levels of antimicrobial resistance and in vivo fitness. Mol Microbiol. 2008;70(2):462-78. Epub 2008/09/03. doi: 10.1111/j.1365-2958.2008.06424.x. PubMed PMID: 18761689; PubMed Central PMCID: PMCPMC2602950.
11. Jerse AE, Sharma ND, Simms AN, Crow ET, Snyder LA, Shafer WM. A gonococcal efflux pump system enhances bacterial survival in a female mouse model of genital tract infection. Infect Immun. 2003;71(10):5576-82. Epub 2003/09/23. doi: 10.1128/iai.71.10.5576-5582.2003. PubMed PMID: 14500476; PubMed Central PMCID: PMCPMC201053.
12. Warner DM, Folster JP, Shafer WM, Jerse AE. Regulation of the MtrC-MtrD-MtrE efflux-pump system modulates the in vivo fitness of Neisseria gonorrhoeae. J Infect Dis. 2007;196(12):1804-12. Epub 2008/01/15. doi: 10.1086/522964. PubMed PMID: 18190261.
13. Lyu M, Moseng MA, Reimche JL, Holley CL, Dhulipala V, Su CC, et al. Cryo-EM Structures of a Gonococcal Multidrug Efflux Pump Illuminate a Mechanism of Drug Recognition and Resistance. mBio. 2020;11(3). Epub 2020/05/28. doi: 10.1128/mBio.00996-20. PubMed PMID: 32457251; PubMed Central PMCID: PMCPMC7251214.

bioRxiv preprint doi: https://doi.org/10.1101/2021.02.24.432727; this version posted February 24, 2021. The copyright holder for this preprint (which was not certified by peer review) is the author/funder. All rights reserved. No reuse allowed without permission.

14. Eicher T, Seeger MA, Anselmi C, Zhou W, Brandstatter L, Verrey F, et al. Coupling of remote alternating-access transport mechanisms for protons and substrates in the multidrug efflux pump AcrB. Elife. 2014;3. Epub 2014/09/24. doi: 10.7554/eLife.03145. PubMed PMID: 25248080; PubMed Central PMCID: PMCPMC4359379.

15. Matsunaga Y, Yamane T, Terada T, Moritsugu K, Fujisaki H, Murakami S, et al. Energetics and conformational pathways of functional rotation in the multidrug transporter AcrB. Elife. 2018;7. Epub 2018/03/07. doi: 10.7554/eLife.31715. PubMed PMID: 29506651; PubMed Central PMCID: PMCPMC5839741.

16. Nakashima R, Sakurai K, Yamasaki S, Nishino K, Yamaguchi A. Structures of the multidrug exporter AcrB reveal a proximal multisite drug-binding pocket. Nature. 2011;480(7378):565-9. Epub 2011/11/29. doi: 10.1038/nature10641. PubMed PMID: 22121023.

17. Su CC, Yin L, Kumar N, Dai L, Radhakrishnan A, Bolla JR, et al. Structures and transport dynamics of a Campylobacter jejuni multidrug efflux pump. Nat Commun. 2017;8(1):171. Epub 2017/08/02. doi: 10.1038/s41467-017-00217-z. PubMed PMID: 28761097; PubMed Central PMCID: PMCPMC5537355.

18. Murakami S, Nakashima R, Yamashita E, Matsumoto T, Yamaguchi A. Crystal structures of a multidrug transporter reveal a functionally rotating mechanism. Nature. 2006;443(7108):173-9. Epub 2006/08/18. doi: 10.1038/nature05076. PubMed PMID: 16915237.

19. Du D, Voss J, Wang Z, Chiu W, Luisi BF. The pseudo-atomic structure of an RND-type tripartite multidrug efflux pump. Biol Chem. 2015;396(9-10):1073-82. Epub 2015/03/25. doi: 10.1515/hsz-2015-0118. PubMed PMID: 25803077.

20. Eicher T, Cha HJ, Seeger MA, Brandstatter L, El-Delik J, Bohnert JA, et al. Transport of drugs by the multidrug transporter AcrB involves an access and a deep binding pocket that are separated by a switch-loop. Proc Natl Acad Sci U S A. 2012;109(15):5687-92. Epub 2012/03/28. doi: 10.1073/pnas.1114944109. PubMed PMID: 22451937; PubMed Central PMCID: PMCPMC3326505.

21. Ramaswamy VK, Vargiu AV, Malloci G, Dreier J, Ruggerone P. Molecular Determinants of the Promiscuity of MexB and MexY Multidrug Transporters of Pseudomonas aeruginosa. Front Microbiol. 2018;9:1144. Epub 2018/06/19. doi: 10.3389/fmicb.2018.01144. PubMed PMID: 29910784; PubMed Central PMCID: PMCPMC5992780.

22. Salomon-Ferrer R, Gotz AW, Poole D, Le Grand S, Walker RC. Routine Microsecond Molecular Dynamics Simulations with AMBER on GPUs. 2. Explicit Solvent Particle Mesh Ewald. J Chem Theory Comput. 2013;9(9):3878-88. Epub 2013/09/10. doi: 10.1021/ct400314y. PubMed PMID: 26592383.

23. D.A. Case IYB-S, S.R. Brozell, D.S. Cerutti, T.E. Cheatham, III, V.W.D. Cruzeiro, T.A. Darden, R.E. Duke, D. Ghoreishi, G. Giambasu, T. Giese, M.K. Gilson, H. Gohlke, A.W. Goetz, D. Greene, R Harris, N. Homeyer, Y. Huang, S. Izadi, A. Kovalenko, R. Krasny, T. Kurtzman, T.S. Lee, S. LeGrand, P. Li, C. Lin, J. Liu, T. Luchko, R. Luo, V. Man, D.J. Mermelstein, K.M. Merz, Y. Miao, G. Monard, C. Nguyen, H. Nguyen, A. Onufriev, F. Pan, R. Qi, D.R. Roe, A. Roitberg, C. Sagui, S. Schott-Verdugo, J. Shen, C.L. Simmerling, J. Smith, J. Swails, R.C. Walker, J. Wang, H. Wei, L. Wilson, R.M. Wolf, X. Wu, L. Xiao, Y. Xiong, D.M. York and P.A. Kollman AMBER 2019. University of California, San Francisco; 2019.

24. Lee J, Cheng X, Swails JM, Yeom MS, Eastman PK, Lemkul JA, et al. CHARMM-GUI Input Generator for NAMD, GROMACS, AMBER, OpenMM, and CHARMM/OpenMM Simulations Using the CHARMM36 Additive Force Field. J Chem Theory Comput. 2016;12(1):405-13. Epub 2015/12/04. doi: 10.1021/acs.jctc.5b00935. PubMed PMID: 26631602; PubMed Central PMCID: PMCPMC4712441.

25. Phillips JC, Braun R, Wang W, Gumbart J, Tajkhorshid E, Villa E, et al. Scalable molecular dynamics with NAMD. J Comput Chem. 2005;26(16):1781-802. Epub 2005/10/14. doi: 10.1002/jcc.20289. PubMed PMID: 16222654; PubMed Central PMCID: PMCPMC2486339.

26. D.A. Case RMB, D.S. Cerutti, T.E. Cheatham, III, T.A. Darden, R.E. Duke, T.J. Giese, H. Gohlke,, A.W. Goetz NH, S. Izadi, P. Janowski, J. Kaus, A. Kovalenko, T.S. Lee, S. LeGrand, P. Li, C., Lin TL,

bioRxiv preprint doi: https://doi.org/10.1101/2021.02.24.432727; this version posted February 24, 2021. The copyright holder for this preprint (which was not certified by peer review) is the author/funder. All rights reserved. No reuse allowed without permission.

R. Luo, B. Madej, D. Mermelstein, K.M. Merz, G. Monard, H. Nguyen, H.T. Nguyen, I., Omelyan AO, D.R. Roe, A. Roitberg, C. Sagui, C.L. Simmerling, W.M. Botello-Smith, J. Swails,, R.C. Walker JW, R.M. Wolf, X. Wu, L. Xiao and P.A. Kollman. AMBER 2016. University of California, San Francisco2016.

27. Case DA, Cheatham TE, 3rd, Darden T, Gohlke H, Luo R, Merz KM, Jr., et al. The Amber biomolecular simulation programs. J Comput Chem. 2005;26(16):1668-88. Epub 2005/10/04. doi: 10.1002/jcc.20290. PubMed PMID: 16200636; PubMed Central PMCID: PMCPMC1989667.
28. Trott O, Olson AJ. AutoDock Vina: improving the speed and accuracy of docking with a new scoring function, efficient optimization, and multithreading. J Comput Chem. 2010;31(2):455-61. Epub 2009/06/06. doi: 10.1002/jcc.21334. PubMed PMID: 19499576; PubMed Central PMCID: PMCPMC3041641.
29. Webb B, Sali A. Comparative Protein Structure Modeling Using MODELLER. Curr Protoc Protein Sci. 2016;86:2 9 1-2 9 37. Epub 2016/11/02. doi: 10.1002/cpps.20. PubMed PMID: 27801516.
30. Hanamoto S, Ogawa F. Predicting the sorption of azithromycin and levofloxacin to sediments from mineral and organic components. Environ Pollut. 2019;255(Pt 1):113180. Epub 2019/09/17. doi: 10.1016/j.envpol.2019.113180. PubMed PMID: 31525559.
31. McFarland JW, Berger CM, Froshauer SA, Hayashi SF, Hecker SJ, Jaynes BH, et al. Quantitative structure-activity relationships among macrolide antibacterial agents: in vitro and in vivo potency against Pasteurella multocida. J Med Chem. 1997;40(9):1340-6. Epub 1997/04/25. doi: 10.1021/jm960436i. PubMed PMID: 9135031.
32. Tim Isgro JP, Marcos Sotomayor, Elizabeth Villa, Hang Yu, David Tanner, Yanxin Liu, Zhe Wu, David Hardy. NAMD Tutorial: Theoretical and Computational Biophysics Group, University of Illinois at Urbana-Champaign; [cited 2021 1/14/2021]. Available from: https://www.ks.uiuc.edu/Training/Tutorials/namd/namd-tutorial-win.pdf.
33. AMBER Histidine residues 2015 [updated 3 May 2020; cited 2021 1/14/2021]. Available from: http://ambermd.org/Questions/HIS.html.
34. Alberts B JA, Lewis J, et al. Molecular Biology of the Cell. 4th Edition. In: Figure 14-32 tIoH-DTiB, editor. New York: Garland; 2002.
35. Vargiu AV, Ramaswamy VK, Malvacio I, Malloci G, Kleinekathofer U, Ruggerone P. Water-mediated interactions enable smooth substrate transport in a bacterial efflux pump. Biochim Biophys Acta Gen Subj. 2018;1862(4):836-45. Epub 2018/01/18. doi: 10.1016/j.bbagen.2018.01.010. PubMed PMID: 29339082.
36. D'Arrigo JS. Screening of membrane surface charges by divalent cations: an atomic representation. Am J Physiol. 1978;235(3):C109-17. Epub 1978/09/01. doi: 10.1152/ajpcell.1978.235.3.C109. PubMed PMID: 696813.
37. Rouquette-Loughlin CE, Reimche JL, Balthazar JT, Dhulipala V, Gernert KM, Kersh EN, et al. Mechanistic Basis for Decreased Antimicrobial Susceptibility in a Clinical Isolate of Neisseria gonorrhoeae Possessing a Mosaic-Like mtr Efflux Pump Locus. mBio. 2018;9(6). Epub 2018/11/30. doi: 10.1128/mBio.02281-18. PubMed PMID: 30482834; PubMed Central PMCID: PMCPMC6282211.
38. Lomize MA, Pogozheva ID, Joo H, Mosberg HI, Lomize AL. OPM database and PPM web server: resources for positioning of proteins in membranes. Nucleic Acids Res. 2012;40(Database issue):D370-6. Epub 2011/09/06. doi: 10.1093/nar/gkr703. PubMed PMID: 21890895; PubMed Central PMCID: PMCPMC3245162.
39. Nikaido H, Takatsuka Y. Mechanisms of RND multidrug efflux pumps. Biochim Biophys Acta. 2009;1794(5):769-81. Epub 2008/11/26. doi: 10.1016/j.bbapap.2008.10.004. PubMed PMID: 19026770; PubMed Central PMCID: PMCPMC2696896.
40. Murzyn K, Rog T, Pasenkiewicz-Gierula M. Phosphatidylethanolamine-phosphatidylglycerol bilayer as a model of the inner bacterial membrane. Biophys J. 2005;88(2):1091-103. Epub 2004/11/24. doi: 10.1529/biophysj.104.048835. PubMed PMID: 15556990; PubMed Central PMCID: PMCPMC1305115.

bioRxiv preprint doi: https://doi.org/10.1101/2021.02.24.432727; this version posted February 24, 2021. The copyright holder for this preprint (which was not certified by peer review) is the author/funder. All rights reserved. No reuse allowed without permission.

41. Wang Z, Fan G, Hryc CF, Blaza JN, Serysheva, II, Schmid MF, et al. An allosteric transport mechanism for the AcrAB-TolC multidrug efflux pump. Elife. 2017;6. Epub 2017/03/30. doi: 10.7554/eLife.24905. PubMed PMID: 28355133; PubMed Central PMCID: PMCPMC5404916.

42. Gaillard P, Carrupt PA, Testa B, Boudon A. Molecular lipophilicity potential, a tool in 3D QSAR: method and applications. J Comput Aided Mol Des. 1994;8(2):83-96. Epub 1994/04/01. doi: 10.1007/BF00119860. PubMed PMID: 7914913.

43. Janganan TK, Bavro VN, Zhang L, Matak-Vinkovic D, Barrera NP, Venien-Bryan C, et al. Evidence for the assembly of a bacterial tripartite multidrug pump with a stoichiometry of 3:6:3. J Biol Chem. 2011;286(30):26900-12. Epub 2011/05/26. doi: 10.1074/jbc.M111.246595. PubMed PMID: 21610073; PubMed Central PMCID: PMCPMC3143649.

44. Lei HT, Chou TH, Su CC, Bolla JR, Kumar N, Radhakrishnan A, et al. Crystal structure of the open state of the Neisseria gonorrhoeae MtrE outer membrane channel. PLoS One. 2014;9(6):e97475. Epub 2014/06/06. doi: 10.1371/journal.pone.0097475. PubMed PMID: 24901251; PubMed Central PMCID: PMCPMC4046963.

45. Schulz R, Vargiu AV, Collu F, Kleinekathofer U, Ruggerone P. Functional rotation of the transporter AcrB: insights into drug extrusion from simulations. PLoS Comput Biol. 2010;6(6):e1000806. Epub 2010/06/16. doi: 10.1371/journal.pcbi.1000806. PubMed PMID: 20548943; PubMed Central PMCID: PMCPMC2883587.

46. Aron Z, Opperman TJ. The hydrophobic trap-the Achilles heel of RND efflux pumps. Res Microbiol. 2018;169(7-8):393-400. Epub 2017/11/18. doi: 10.1016/j.resmic.2017.11.001. PubMed PMID: 29146106; PubMed Central PMCID: PMCPMC5949246.

47. Vargiu AV, Nikaido H. Multidrug binding properties of the AcrB efflux pump characterized by molecular dynamics simulations. Proc Natl Acad Sci U S A. 2012;109(50):20637-42. Epub 2012/11/24. doi: 10.1073/pnas.1218348109. PubMed PMID: 23175790; PubMed Central PMCID: PMCPMC3528587.

48. Humphrey W, Dalke A, Schulten K. VMD: visual molecular dynamics. J Mol Graph. 1996;14(1):33-8, 27-8. Epub 1996/02/01. doi: 10.1016/0263-7855(96)00018-5. PubMed PMID: 8744570.

49. Jo S, Kim T, Iyer VG, Im W. CHARMM-GUI: a web-based graphical user interface for CHARMM. J Comput Chem. 2008;29(11):1859-65. Epub 2008/03/21. doi: 10.1002/jcc.20945. PubMed PMID: 18351591.

50. Brooks BR, Brooks CL, 3rd, Mackerell AD, Jr., Nilsson L, Petrella RJ, Roux B, et al. CHARMM: the biomolecular simulation program. J Comput Chem. 2009;30(10):1545-614. Epub 2009/05/16. doi: 10.1002/jcc.21287. PubMed PMID: 19444816; PubMed Central PMCID: PMCPMC2810661.

51. Morris GM, Huey R, Lindstrom W, Sanner MF, Belew RK, Goodsell DS, et al. AutoDock4 and AutoDockTools4: Automated docking with selective receptor flexibility. J Comput Chem. 2009;30(16):2785-91. Epub 2009/04/29. doi: 10.1002/jcc.21256. PubMed PMID: 19399780; PubMed Central PMCID: PMCPMC2760638.

52. Grant BJ, Rodrigues AP, ElSawy KM, McCammon JA, Caves LS. Bio3d: an R package for the comparative analysis of protein structures. Bioinformatics. 2006;22(21):2695-6. Epub 2006/08/31. doi: 10.1093/bioinformatics/btl461. PubMed PMID: 16940322.

53. Goddard TD, Huang CC, Meng EC, Pettersen EF, Couch GS, Morris JH, et al. UCSF ChimeraX: Meeting modern challenges in visualization and analysis. Protein Sci. 2018;27(1):14-25. Epub 2017/07/16. doi: 10.1002/pro.3235. PubMed PMID: 28710774; PubMed Central PMCID: PMCPMC5734306.

54. O'Boyle NM, Banck M, James CA, Morley C, Vandermeersch T, Hutchison GR. Open Babel: An open chemical toolbox. J Cheminform. 2011;3:33. Epub 2011/10/11. doi: 10.1186/1758-2946-3-33. PubMed PMID: 21982300; PubMed Central PMCID: PMCPMC3198950.

55. Rostkowski M, Olsson MH, Sondergaard CR, Jensen JH. Graphical analysis of pH-dependent properties of proteins predicted using PROPKA. BMC Struct Biol. 2011;11:6. Epub 2011/01/29. doi: 10.1186/1472-6807-11-6. PubMed PMID: 21269479; PubMed Central PMCID: PMCPMC3038139.

bioRxiv preprint doi: https://doi.org/10.1101/2021.02.24.432727; this version posted February 24, 2021. The copyright holder for this preprint (which was not certified by peer review) is the author/funder. All rights reserved. No reuse allowed without permission.

56. Kong FY, Rupasinghe TW, Simpson JA, Vodstrcil LA, Fairley CK, McConville MJ, et al. Pharmacokinetics of a single 1g dose of azithromycin in rectal tissue in men. PLoS One. 2017;12(3):e0174372. Epub 2017/03/30. doi: 10.1371/journal.pone.0174372. PubMed PMID: 28350806; PubMed Central PMCID: PMCPMC5370104.

57. McCormick JW, Vogel PD, Wise JG. Multiple Drug Transport Pathways through Human P-Glycoprotein. Biochemistry. 2015;54(28):4374-90. Epub 2015/07/10. doi: 10.1021/acs.biochem.5b00018. PubMed PMID: 26125482; PubMed Central PMCID: PMCPMC4527178.

58. Wise JG. Catalytic transitions in the human MDR1 P-glycoprotein drug binding sites. Biochemistry. 2012;51(25):5125-41. Epub 2012/06/12. doi: 10.1021/bi300299z. PubMed PMID: 22647192; PubMed Central PMCID: PMCPMC3383123.

59. Wang J, Wang W, Kollman PA, Case DA. Automatic atom type and bond type perception in molecular mechanical calculations. J Mol Graph Model. 2006;25(2):247-60. Epub 2006/02/07. doi: 10.1016/j.jmgm.2005.12.005. PubMed PMID: 16458552.

60. Wang J, Wolf RM, Caldwell JW, Kollman PA, Case DA. Development and testing of a general amber force field. J Comput Chem. 2004;25(9):1157-74. Epub 2004/04/30. doi: 10.1002/jcc.20035. PubMed PMID: 15116359.

61. Dolinsky TJ, Czodrowski P, Li H, Nielsen JE, Jensen JH, Klebe G, et al. PDB2PQR: expanding and upgrading automated preparation of biomolecular structures for molecular simulations. Nucleic Acids Res. 2007;35(Web Server issue):W522-5. Epub 2007/05/10. doi: 10.1093/nar/gkm276. PubMed PMID: 17488841; PubMed Central PMCID: PMCPMC1933214.

62. Baker NA, Sept D, Joseph S, Holst MJ, McCammon JA. Electrostatics of nanosystems: application to microtubules and the ribosome. Proc Natl Acad Sci U S A. 2001;98(18):10037-41. Epub 2001/08/23. doi: 10.1073/pnas.181342398. PubMed PMID: 11517324; PubMed Central PMCID: PMCPMC56910.

63. Dolinsky TJ, Nielsen JE, McCammon JA, Baker NA. PDB2PQR: an automated pipeline for the setup of Poisson-Boltzmann electrostatics calculations. Nucleic Acids Res. 2004;32(Web Server issue):W665-7. Epub 2004/06/25. doi: 10.1093/nar/gkh381. PubMed PMID: 15215472; PubMed Central PMCID: PMCPMC441519.

64. ACE and JChem acidity and basicity Calculator. ACE UKY-4.0

ed. https://epoch.uky.edu/ace/public/pKa.jsp: Marvin JS, ChemAxon.

65. Daina A, Michielin O, Zoete V. SwissADME: a free web tool to evaluate pharmacokinetics, drug-likeness and medicinal chemistry friendliness of small molecules. Sci Rep. 2017;7:42717. Epub 2017/03/04. doi: 10.1038/srep42717. PubMed PMID: 28256516; PubMed Central PMCID: PMCPMC5335600.

bioRxiv preprint doi: https://doi.org/10.1101/2021.02.24.432727; this version posted February 24, 2021. The copyright holder for this preprint (which was not certified by peer review) is the author/funder. All rights reserved. No reuse allowed without permission.

Supporting information

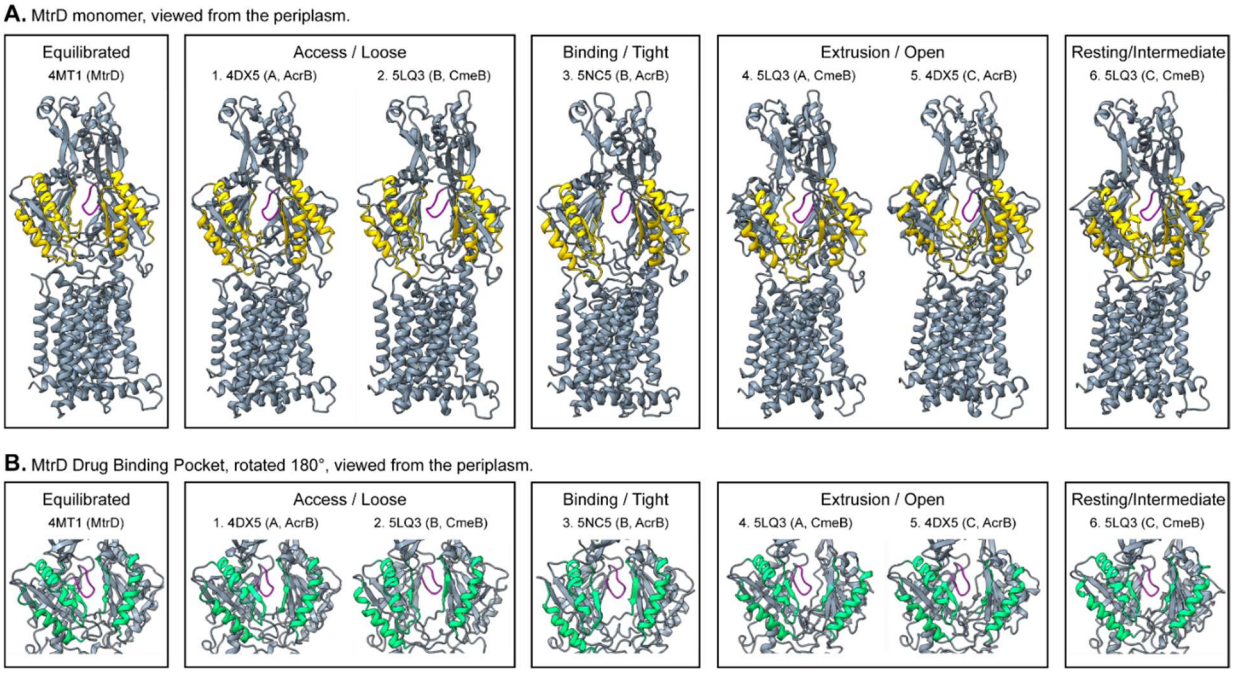

S1 Fig. Modeling a Putative Catalytic Transport Cycle of MtrD using MtrD Homologues. (A) The MtrD monomer viewed from the periplasm, with helices of the Access Pocket colored yellow for visibility, and the G-Loop colored magenta. Here we show all of the structures of MtrD homologues, in order, that were used to model a putative catalytic efflux cycle of MtrD with TMD simulations. The overall title of the stage of transport – Access, Binding, Extrusion, Transition (Intermediate) is above the structures used; the PDB ID of the structure is numbered in all caps, the specific chain of the PDB, as well as the name of the source protein, are in parentheses. (B) The periplasmic cleft of the MtrD monomer viewed from the back, or from the center of the transporter. Helices of the Deep Pocket are colored green, the G-Loop is in magenta. These images are the same structures as in (A) but rotated 180° and viewed from the back.

bioRxiv preprint doi: https://doi.org/10.1101/2021.02.24.432727; this version posted February 24, 2021. The copyright holder for this preprint (which was not certified by peer review) is the author/funder. All rights reserved. No reuse allowed without permission.

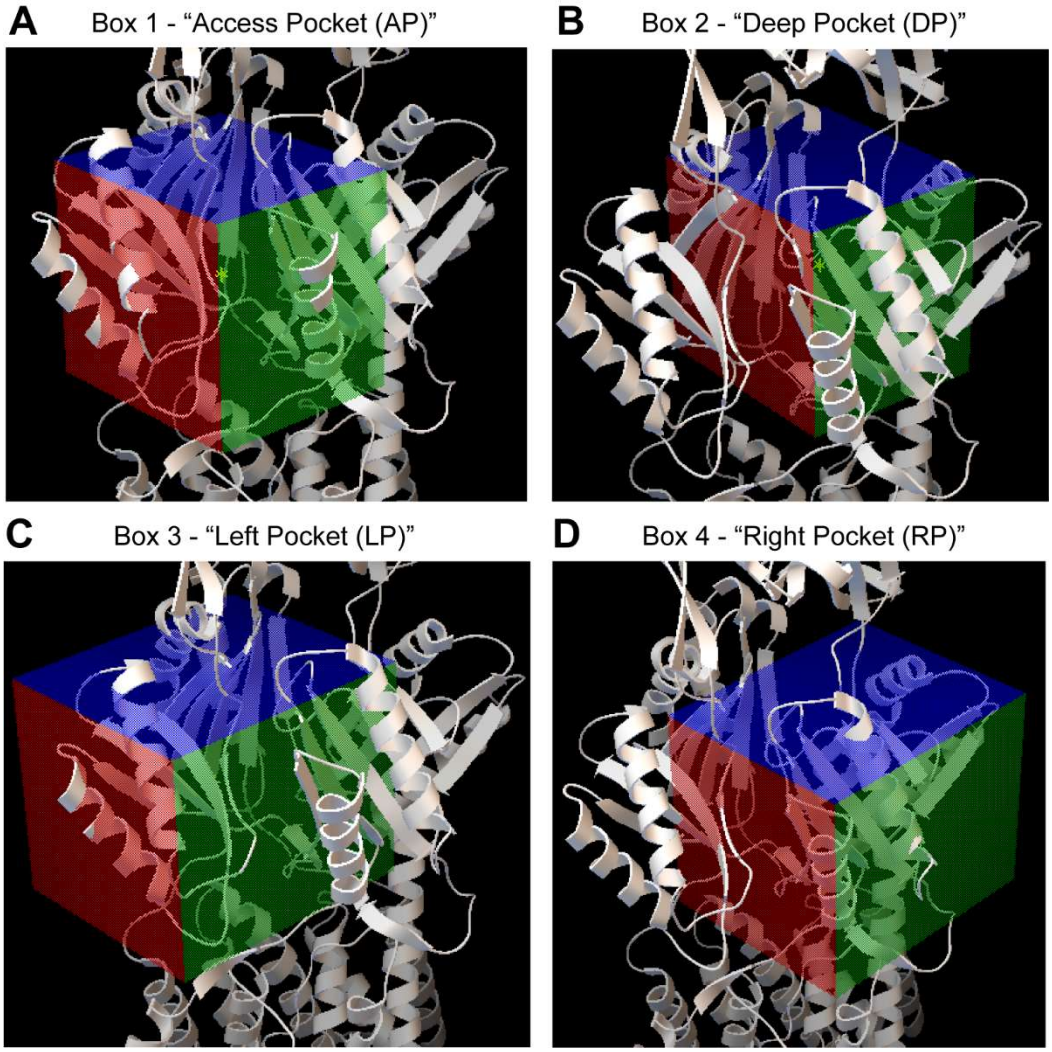

S2 Fig. Docking Search Areas used for Docking Streptomycin and Azithromycin to the Periplasmic Cleft of MtrD.

Docking search areas were designed with a spacing of 1 angstrom using Autodock Tools; docking search areas were also chosen with significant overlap to ensure that the periplasmic cleft was adequately sampled. Docking experiments were performed with *Autodock Vina* and an exhaustiveness of 128 (default is 8). (A-B) The dimensions of the Access Pocket and Deep Pocket docking boxes are 26 x 30 x 28. (C-D) The dimensions of the Left Pocket and Right Pocket docking boxes are 36 x 30 x 30. Streptomycin and Azithromycin were docked against the periplasmic cleft using each of these four docking boxes, as described in Methods.

bioRxiv preprint doi: https://doi.org/10.1101/2021.02.24.432727; this version posted February 24, 2021. The copyright holder for this preprint (which was not certified by peer review) is the author/funder. All rights reserved. No reuse allowed without permission.

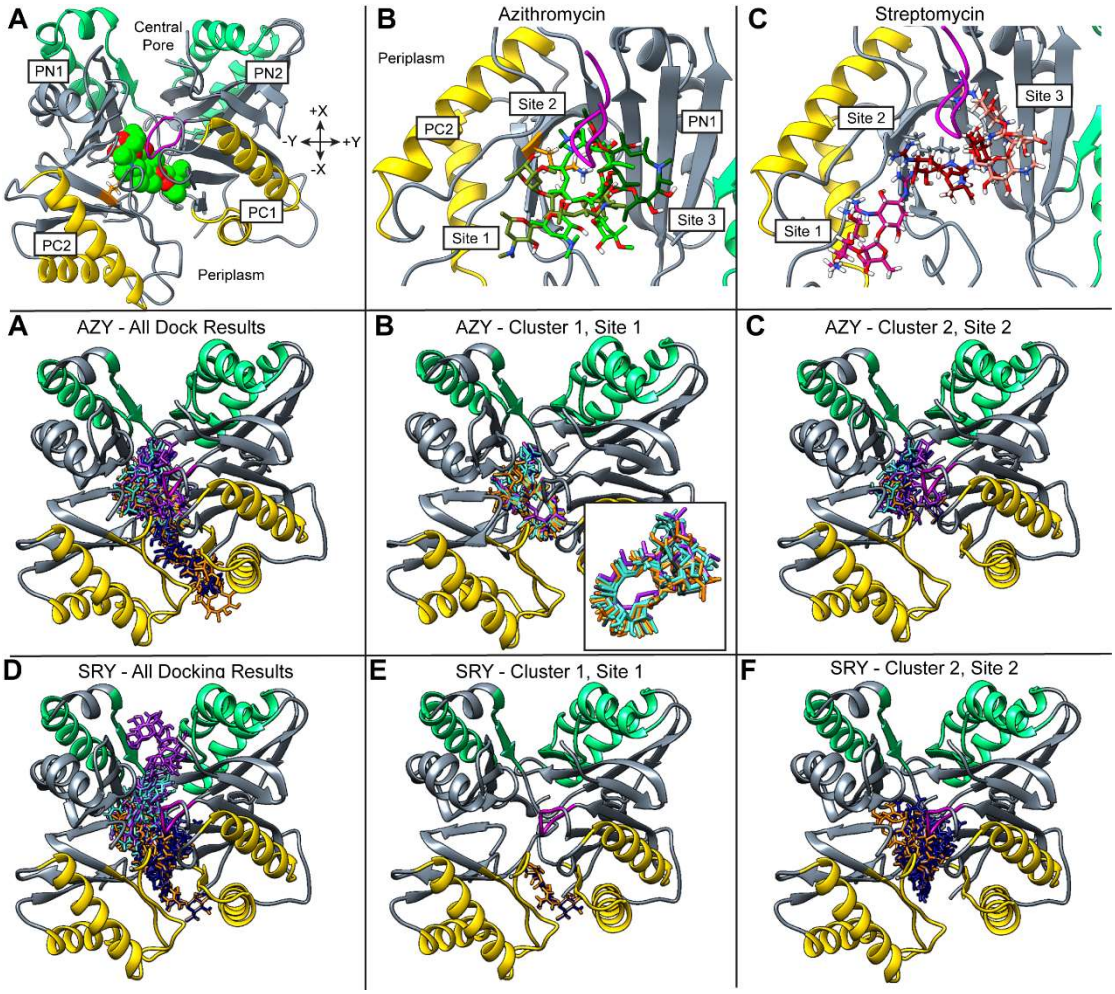

S3 Fig. Ligand Docking Poses and Selection of Start Sites for TMD Simulations.
Panels (A-H) show the periplasmic cleft of MtrD viewed from the top (i.e. periplasm) down, with helices of the Access Pocket colored yellow, and helices of the Deep Pocket colored green, for aid in reader orientation. The Access Pocket is exposed to the periplasm, and the Deep Pocket opens into the interior of the MtrD transporter. All resultant docking poses of streptomycin (SRY) and azithromycin (AZY) are shown in stick representation. (A) All docking results of AZY overlaid, from all four dock boxes shown in S2 Fig. (B) Docking cluster 1, this was the most occupied cluster for azithromycin, with a zoom-in showing the overlapping poses; this cluster was the basis for Site 1. (C) the second most occupied docking cluster of azithromycin, this cluster was the basis for Site 2. (D) the third most occupied cluster; this cluster was the basis for Site 3. (E) All docking results of SRY overlaid from all four dock boxes. (F) The Access Pocket cluster that was the basis for Site 1. (G) the second most occupied cluster; this cluster was the basis for Site 2. (H) the third most occupied cluster, this was the basis for Site 3.

bioRxiv preprint doi: https://doi.org/10.1101/2021.02.24.432727; this version posted February 24, 2021. The copyright holder for this preprint (which was not certified by peer review) is the author/funder. All rights reserved. No reuse allowed without permission.

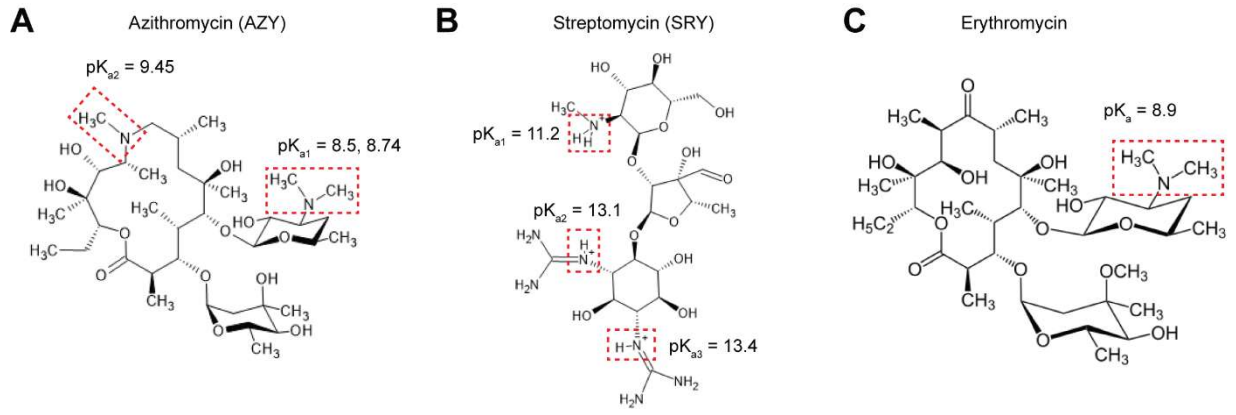

S4 Fig. Structures of Azithromycin (AZY), Streptomycin (SRY), and Erythromycin
Panels show the molecular structure, protonation sites, and relative pKas of **A)** azithromycin (AZY), **B)** streptomycin (SRY), and **C)** erythromycin [31, 64]. Azithromycin and Erythromycin are both macrolides, and are also substrates of MtrD [9, 13]. Structures were sourced from the PubChem database, and pKas were sourced from [31, 64].

S1 Table. Predicted Molecular Characteristics of AZY, SRY, and Erythromycin.

Molecule	Molecular Weight (g/mol)	Topological Polar Surface Area (TPSA, Å^2)	Consensus Log $P_{o/w}$	Water Solubility (Log *S*)	Number of H-bond acceptors	Number of H-bond Donors
SRY	548.6	344.23	-7.36	Highly soluble	12	14
AZY_{neu}	734.96	191.08	1.15	Poorly soluble	14	6
AZY_{h1}	735.97	191.28	0.13	Poorly soluble	13	7
AZY_{h2}	736.97	191.48	-0.89	Poorly soluble	12	8
ERY_{neu}	733.92	193.91	1.99	Soluble	14	5
ERY_{h1}	734.93	195.11	0.97	Soluble	13	6

The physicochemical descriptors and properties of the three different protonation states of AZY, the single protonation state of SRY, and the two protonation states of erythromycin, were calculated using the SWISS-ADME server *[65]*. The consensus Log P is the average of the calculated LogP using five different methods. The Log S indicates the predicted solubility in water. SWISS-ADME presents three different predictions of Log S each using different methodology, with the potential classifications 'highly soluble', 'soluble', and 'poorly soluble'. For each form of AZY, 2/3 methods predicted "poorly soluble", the remaining method (SILICOS-IT) predicted "soluble". For SRY, 2/3 methods predicted "highly soluble", the remaining method (SILICOS-IT) predicted "soluble". The Topological Polar Surface Area (TPSA) indicates the surface sum over all polar atoms in the respective molecule in Å^2; as TPSA increases, hydrophilicity increases.

bioRxiv preprint doi: https://doi.org/10.1101/2021.02.24.432727; this version posted February 24, 2021. The copyright holder for this preprint (which was not certified by peer review) is the author/funder. All rights reserved. No reuse allowed without permission.

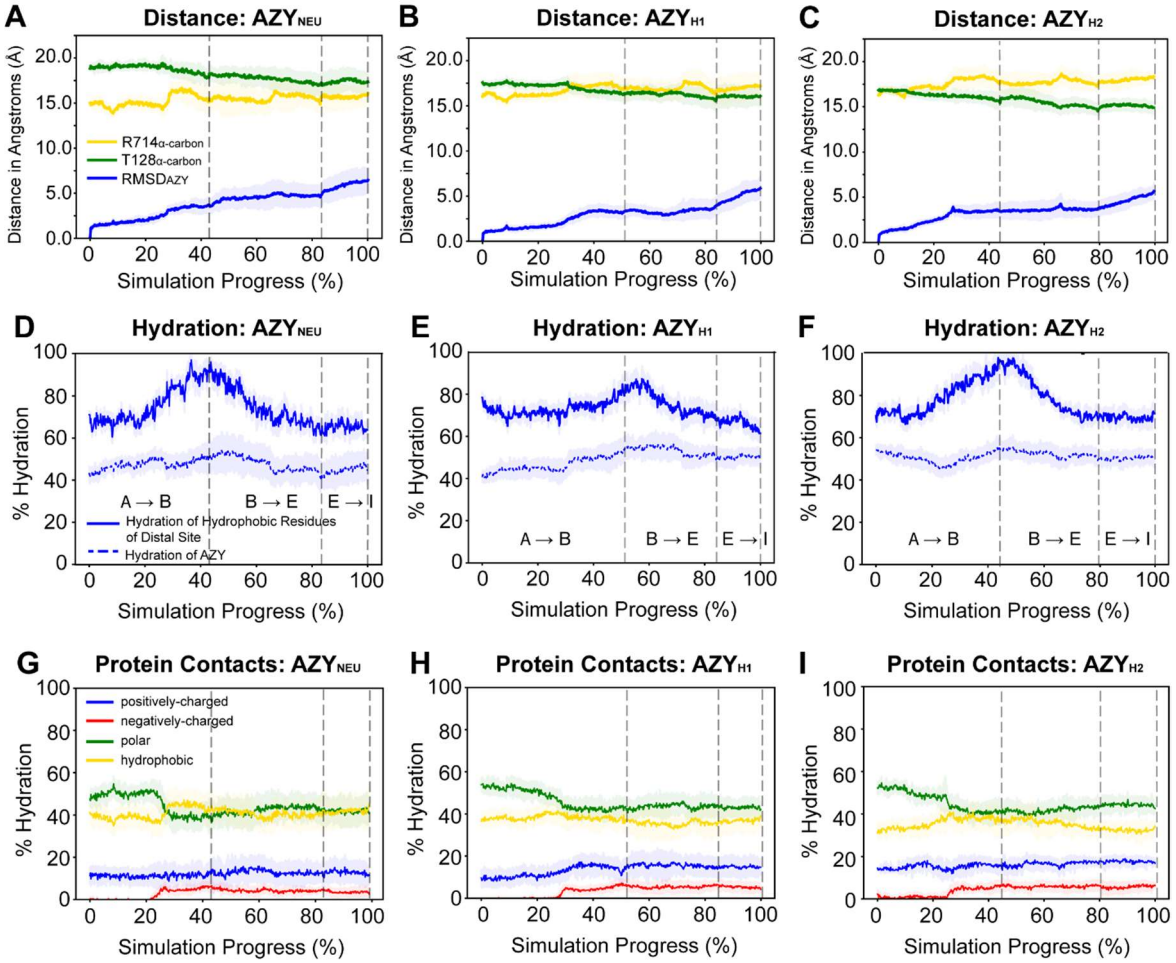

S5 Fig. Results of the "Non-Transport" Cluster – TMD Simulations of AZY at Site 1. A-C) show the RMSD of AZY from its starting position over time, and the distance between the center of mass of AZY and the α-carbons of T128 or R714 in the periplasmic cleft. In contrast to the results in Fig 3, notice that the $RMSD_{AZY}$ is < 10 Å, and the distance between AZY and the two checkpoints within the cleft (R714, T128) does not change as much as in the 'Transport' cluster. **D-F)** show the hydration of AZY or of the hydrophobic residues in the distal binding site over the course of the simulation. Percent (%) hydration is calculated as the number of molecules within 4 Å of AZY or the hydrophobic residues, divided by the total number of water molecules needed to hydrate them completely. **G-I)** show the nature of protein-AZY contacts over the course of the simulation. In **A-I)**, data are presented as the mean with ± one standard deviation in shading. Dashed grey lines indicate structural checkpoints, and timepoints between the lines indicate structural transitions.

bioRxiv preprint doi: https://doi.org/10.1101/2021.02.24.432727; this version posted February 24, 2021. The copyright holder for this preprint (which was not certified by peer review) is the author/funder. All rights reserved. No reuse allowed without permission.

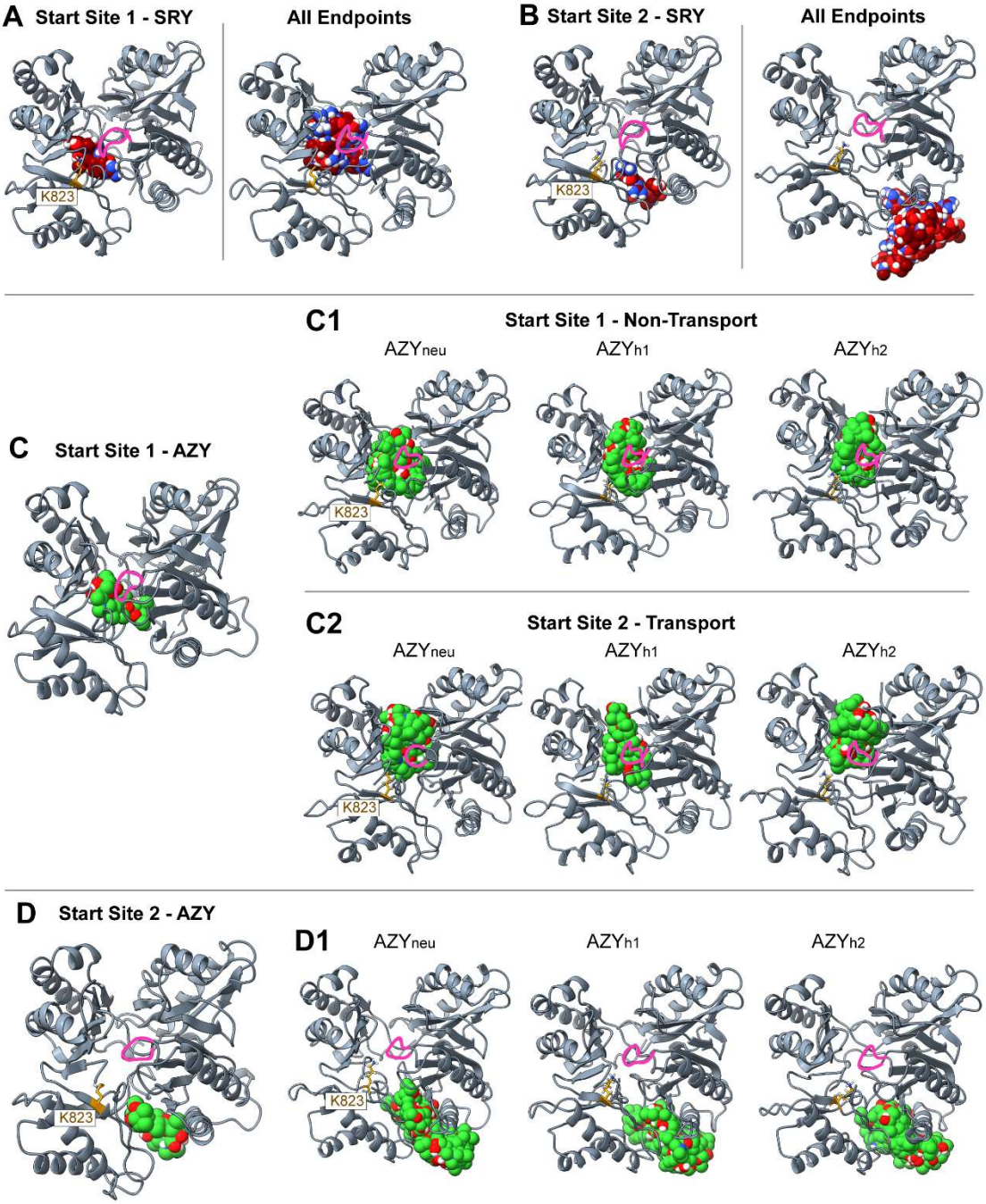

S6 Fig. All Simulation Starting Points and Ending Points for TMD Simulations with AZY and SRY. All panels show the periplasmic cleft of MtrD viewed from the top down. The G-Loop is outlined in magenta, K823 is orange and in licorice representation, SRY and AZY are in spacefill representation, AZY is in lime green, and SRY is in maroon. Panels **A) and B)** show the starting position of SRY at **A)** Starting Site 1 and **B)** Starting Site 2. The left image shows SRY in its starting position. The right image shows all of the ending positions of SRY superimposed, n = 20 simulations per starting site. **C)** shows the results of simulations with AZY from Starting Site 1; **C1)** shows the ending position of AZY in all 'Non-Transport' trajectories, and **C2)** shows the ending position of AZY in all 'Transport' trajectories. **D)** shows the results of simulations with AZY from Starting Site 2; **D1)** shows the ending position of AZY divided by protonation state, n = 20 simulations per ligand. Note that, in contrast to the results of SRY at Site 2 (Panel B), AZY is still within the entrance of the periplasmic cleft in the majority of the simulations, whereas SRY had exited the periplasmic cleft completely.

bioRxiv preprint doi: https://doi.org/10.1101/2021.02.24.432727; this version posted February 24, 2021. The copyright holder for this preprint (which was not certified by peer review) is the author/funder. All rights reserved. No reuse allowed without permission.

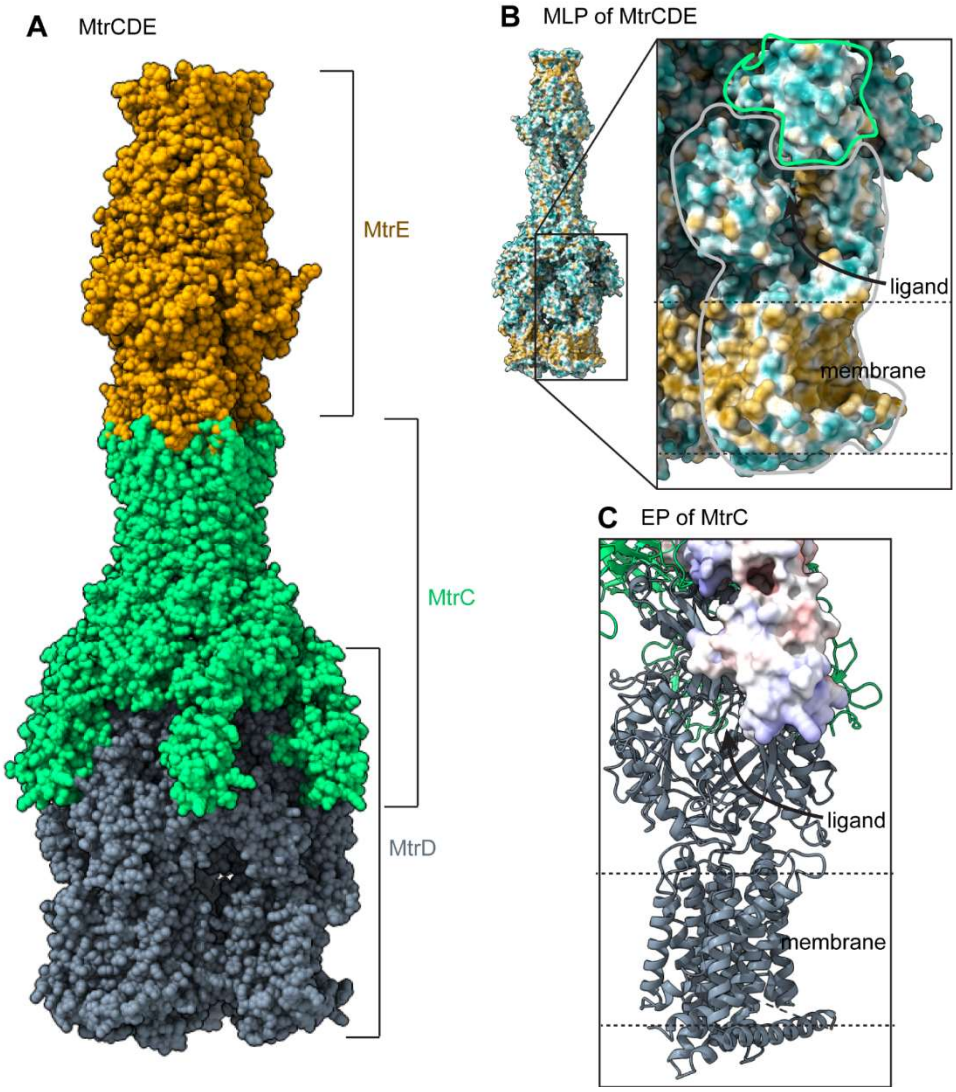

S7 Fig. Homology Model of MtrCDE. *A) shows our fully assembled homology model of MtrCDE; the model was assembled using the 5NG5 structure of AcrAB-TolC as a structural template (see Methods) [41]. B) The MLP (molecular lipophilicity potential) of MtrCDE; the zoom-in panel shows the interface between MtrC (outlined in green) and MtrD (outlined in grey). C) The electrostatic potential (EP) surfaces of MtrC calculated by the PDB2PQR server. The MtrC-MtrD interface (that could potentially contact ligands) contains mostly neutral MLP and EP isosurfaces.*

bioRxiv preprint doi: https://doi.org/10.1101/2021.02.24.432727; this version posted February 24, 2021. The copyright holder for this preprint (which was not certified by peer review) is the author/funder. All rights reserved. No reuse allowed without permission.

1338

A **Key: RND Pump Structures and Details**

PDB (chain)	Pump	Resolution (Angstroms)	Conformation of chain	Ligand in Binding Protomer?
4MT1 (A)	MtrD	3.54	Access	
6VKT (A)	$MtrD_{CR.103}$	2.72	Access	
6VKS (A)	$MtrD_{CR.103}$	3.02	Access	
6VKT (B)	$MtrD_{CR.103}$	2.72	Binding	Erythromycin
6VKS (B)	$MtrD_{CR.103}$	3.02	Binding	Ampicillin
6VKT (C)	$MtrD_{CR.103}$	2.72	Extrusion	
6VKS (C)	$MtrD_{CR.103}$	3.02	Extrusion	
4DX5 (A)	AcrB	1.90	Access	
5LQ3 (B)	CmeB	3.55	Access	
5NC5 (B)	AcrB	3.20	Binding	Puromycin
5LQ3 (A)	CmeB	3.55	Extrusion	
4DX5 (C)	AcrB	1.90	Extrusion	
5LQ3 (C)	CmeB	3.55	Intermediate	

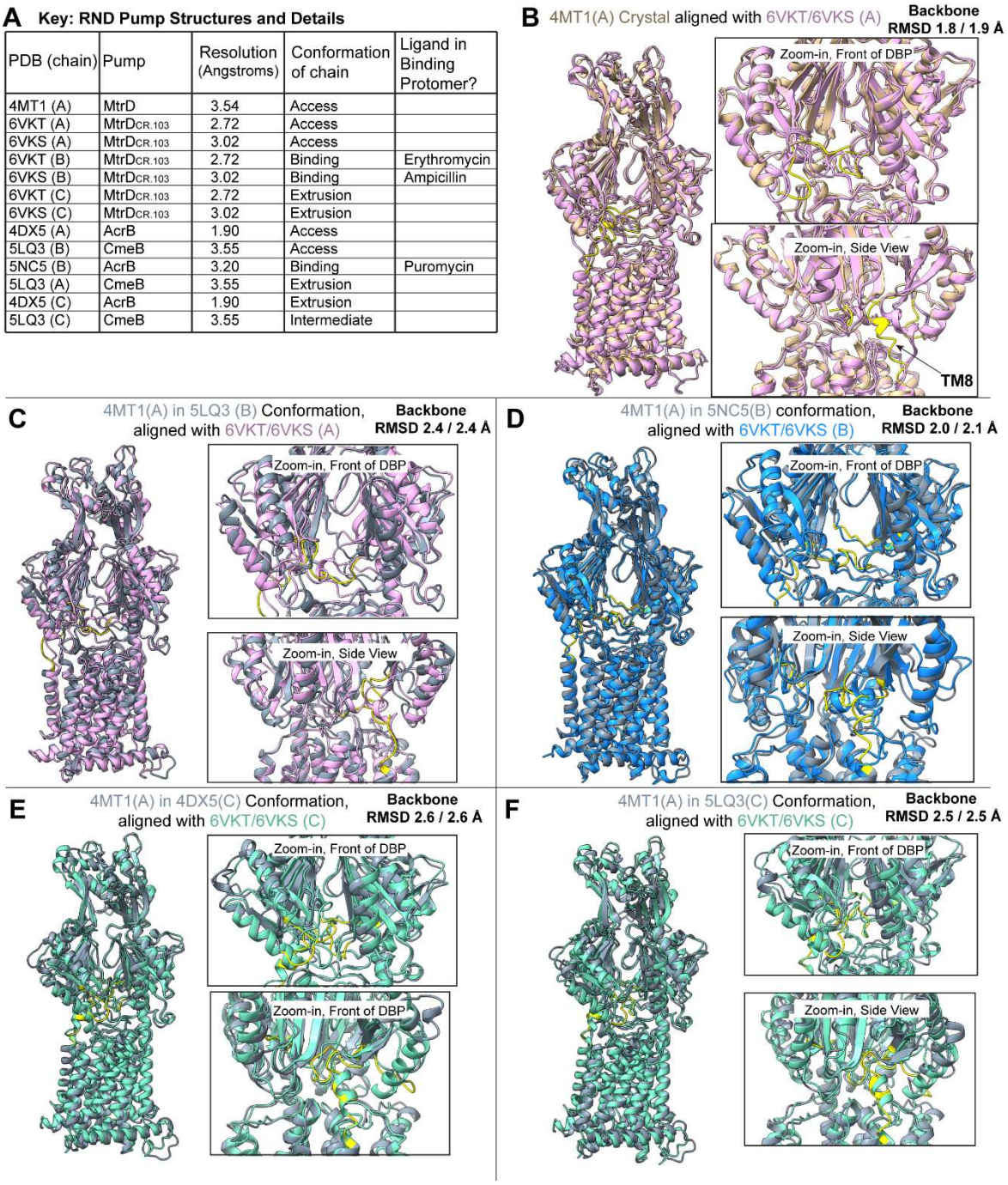

1339

1340 **S8 Fig. Alignment and Backbone RMSD Comparison of MtrD with Known Structures of**
1341 **Homologous RND Transporters and with $MtrD_{CR103}$.** A) A table showing the PDB ID (chain ID), pump
1342 of origin, resolution, conformational class, and ligand present (if any). B) MtrD (4MT1, tan) aligned with
1343 the Access protomers of 6VKT/6VKS of $MtrD_{CR103}$ (purple). C) MtrD post-TMD guidance to the Access
1344 conformation of CmeB (gray), aligned with the Access protomers of 6VKT/6VKS (purple). D) MtrD post-
1345 TMD guidance to the Binding conformation of AcrB (gray), aligned with the Binding protomers of
1346 6VKT/6VKS (blue). E) MtrD post-TMD guidance to the Extrusion conformation of AcrB (gray), aligned
1347 with the Extrusion protomers of 6VKT/6VKS (green). F) MtrD post-TMD guidance to the "Intermediate"
1348 conformation of CmeB (gray), aligned with the Extrusion protomers of 6VKT/6VKS (green). Alignments
1349 and RMSD calculations were performed with the RMSD Trajectory tool in VMD [48].